The effect of greenhouse-gas-induced changes in SST on the seasonality of tropical precipitation

John G. Dwyer *

Columbia University, Department of Applied Physics and Applied Mathematics, New York, NY

Michela Biasutti

Lamont-Doherty Earth Observatory, Columbia University, Palisades, NY

Adam H. Sobel

Department of Applied Physics and Applied Mathematics, Department of Earth and Environmental Sciences, and Lamont-Doherty Earth Observatory, Columbia University, New York, NY

* *Corresponding author address:* John G. Dwyer, Department of Applied Physics and Applied Mathematics, Columbia University, 500 W. 120th St., New York, NY 10027.

E-mail: jgd2102@columbia.edu

ABSTRACT

CMIP5 models project changes to the seasonality of both tropical sea surface temperature (SST) and precipitation when forced by an increase in greenhouse gases. Nearly all models project an amplification and a phase delay of the annual cycle for both quantities, indicating a greater annual range and extrema reached later in the year. We detail these changes and investigate the nature of the seasonal precipitation changes in an AGCM. In response to a prescribed SST with a uniformly higher annual mean temperature, we find a strengthened annual cycle of precipitation due to enhanced vertical moisture advection, and we find a delay to the timing of peak precipitation, consistent with a delay to the timing of the circulation. A budget analysis of this simulation indicates a large degree of similarity with the CMIP5 results. In the second experiment, we change only the seasonal characteristics of SST. For an amplified annual cycle of SST we find an amplified annual cycle of precipitation, while for a delayed SST we find a delayed annual cycle of precipitation. Additionally, there are cross-effects: the phase of SST affects the amplitude of precipitation and the amplitude of SST affects the phase of precipitation. Assuming that the seasonal changes of precipitation in the CMIP5 models are entirely due to SST effects and that ocean feedbacks are not important, our AGCM simulations suggest that the annual mean SST warming can explain around 90% of the amplitude increase and 60% of the phase delay of precipitation in the CMIP5 models with the remainder due to seasonal changes in SST.

1. Introduction

The seasonal cycle of tropical precipitation, primarily characterized by the monsoons and the meridional movement of the ITCZ, is responsible for much of the variance in global precipitation. Even relatively small changes in the annual cycle of tropical precipitation may have a large impact, both globally and locally. For example, they can affect the timing and quantity of latent heat release and energy transport, which can also affect the general circulation. Changes in monsoonal timing have large regional implications due to the dependence of many agricultural and pastoral communities on rainfall.

Nearly all of the models in the World Climate Research Programme's (WCRP's) Coupled Model Intercomparison Project phase 3 (CMIP3) multi-model dataset (Meehl et al. 2007) project consistent changes to the annual cycle of SST and precipitation in simulations with increased greenhouse gases: a phase delay and an amplification of the annual cycles of tropical precipitation and SST (Chou et al. 2007; Tan et al. 2008; Biasutti and Sobel 2009; Sobel and Camargo 2011; Seth et al. 2011; Dwyer et al. 2012). CMIP5 (Taylor et al. 2011) models show changes of the same sign due to greenhouse gases, which we discuss in Section 3 and which have been documented elsewhere (Biasutti 2013; Seth et al. 2013; Huang et al. 2013). Averaged over the tropical ocean for CMIP5, the changes to the annual cycle are relatively small: a 1 day delay and a 4% amplitude increase for SST and a 3 day delay and a 16% amplitude increase for precipitation. But these changes are consistent across models.

We are interested in the question of what modifies the seasonal cycles of both precipitation and surface temperature in the greenhouse-gas forced, fully coupled models. In this paper we address a more limited question: given a change in the annual mean or annual cycle of SST, what is the response of the annual cycle of precipitation and how does this relate to changes in the coupled models? Using an AGCM forced with SST presents a simple framework to evaluate this question, but there are drawbacks to this approach. Prescribing SST eliminates feedbacks between the ocean and atmosphere that are present in the real climate and coupled models (Fu and Wang 2004; Kitoh and Arakawa 1999). Despite this, given the observed SST and radiative forcings, AGCMs capture the annual precipitation anomalies over land and for the tropics over all, though there is some discrepancy over ocean (Liu et al. 2012). Similar studies where the annual cycle of SST was modified or suppressed have been carried out to study the effect of SST on the Asian summer monsoon (Shukla and Fennessy 1994), the equatorial Atlantic and Pacific (Li and Philander 1997), precipitation in the Amazon basin (Fu et al. 2001), and precipitation in the tropical Atlantic (Biasutti et al. 2003, 2004).

If the mean or seasonal changes in SST can directly force seasonality changes in precipitation in the AGCM, this suggests that the same mechanism might be operating in the greenhouse gas forced, coupled models. While this study cannot rule out alternative mechanisms for the seasonality changes of precipitation in the coupled models, it demonstrates that changes to the annual mean and annual cycle of SST are each a sufficient (though not necessarily a necessary) condition for affecting the seasonal cycle of precipitation. Moreover, we find that increasing the annual mean SST alone – and not changing its seasonality – in an AGCM produces an amplitude increase and a phase delay of tropical precipitation with similar magnitude and structure to the coupled models.

Ultimately, greenhouse gases are responsible for the changes to both SST and precipitation in the coupled models. And while our results suggest that precipitation is responding to changes to SST, the mechanism by which greenhouse gases affect the seasonality of SST is not yet clear. Earlier research has suggested a link to the surface fluxes (specifically latent heat flux), which may be due to changes in the Hadley Circulation (Sobel and Camargo 2011; Dwyer et al. 2012).

In the following section we describe the methods, AGCM, experimental design, and sensitivity of the results to our methods. Next in Section 3 we describe the annual mean and seasonal changes to SST and precipitation in the CMIP5 models, which motivates the modeling studies. In Section 4 and 5 we describe and interpret the results of our simulations in which we uniformly increase the SST and changed the seasonality of SST, respectively. We discuss our results in Section 6 before concluding in Section 7.

2. Methods and Experimental Design

We reproduce the CMIP3 results of an amplitude increase and a phase delay for SST and precipitation in the tropics (25°S–25°N) with 35 of the CMIP5 models for which monthly precipitation and surface temperature data for both the historical simulation and RCP8.5 scenario are available. The RCP8.5 simulation represents a high greenhouse gas emission scenario with a year 2100 radiative forcing of around 8.5 W m^{-2} relative to pre-industrial conditions (Taylor et al. 2011). A full list of models in this study is included in Table 1.

For our modeling simulations, we use the atmospheric component of the National Center for Atmospheric Research (NCAR) Community Climate Systems Model, version 4 (CCSM4) (Gent et al. 2011) at the standard resolution ($1.9° \times 2.5°$). To create a control simulation, we run the model for 20 years with monthly-averaged, climatological SST determined from the Hadley Center and NOAA for the 1982–2001 observation period (Hurrell et al. 2008). The perturbed simulations were run for 10 years, sufficiently long to characterize the annual cycle of precipitation. The only change we made in the perturbed simulations was to either alter the mean or the annual cycle of SST. Land temperatures were free to adjust on their own and the atmospheric chemical composition was the same between simulations.

We use two methods to calculate the seasonal characteristics of temperature and precipitation. The first is to Fourier transform data to directly obtain the phase and amplitude of the annual harmonic; this decomposition can be performed pointwise. The second method is Empirical Orthogonal Function (EOF) analysis, which extracts patterns of coherent variability in the data (Kutzbach 1967). The dominant spatial pattern (EOF1) explains 85% of tropical SST and 70% of tropical precipitation, and reverses its sign across the equator. By fitting a sinusoid to the principal component (PC) associated with the annual cycle, PC1, we obtain the seasonal characteristics (Biasutti and Sobel 2009; Dwyer et al. 2012). Any change to PC1 of precipitation can be interpreted as a change in the timing or strength of the ITCZ movement or monsoonal precipitation (Figure 1(a)), assuming that EOF1 changes little, an assumption we address below.

To create the SST forcing for the uniform warming (UW) experiment, we simply adjust the climatological SST by a fixed amount (3 K) for every month and at every spatial grid point. For the seasonality experiment, we modify the phase and amplitude of the SST forcing by first calculating the phase and amplitude of the annual harmonic of the control SST at each grid point using a Fourier transform and then either shifting the phase or amplifying the amplitude of the first harmonic before performing an inverse Fourier transform.

Alternatively, we could change the seasonality of all harmonics, instead of only the first. We test this effect by comparing two forced simulations differing only in the number of harmonics that are shifted. The difference between the two simulations is small for SST, precipitation and other climate variables. We also tested the effect of changing the seasonality of sea ice in addition to SST. This led to large near-surface air temperature differences at high latitudes, but only small changes in precipitation at low latitudes.

In order to interpret the changes to PC1 as a shift or amplification of the timing of tropical precipitation, we require that the leading EOF pattern of each experiment be similar to that of the control. In the simulations we perform, the EOF patterns are very similar. Figures 1(b) and (c) show the EOF1 pattern of precipitation for a phase delay of 15 days and an amplitude increase of 25%, respectively. The effect of the phase of SST on the EOF1 pattern of precipitation is small everywhere. Changing the amplitude of SST has a slightly larger effect on the EOF1 pattern of precipitation – it becomes stronger in some regions and weaker in others. Because the EOF1 patterns are normalized to the same global variance, an increased amplitude of precipitation will be expressed through the amplitude of PC1, not EOF1. We also verify our results by projecting the precipitation data for each forced run onto EOF1 of the control run and find only small differences from the standard method of projecting the precipitation data onto its own EOF1, leaving our conclusions unchanged.

3. CMIP5 Results

In response to increased greenhouse gases in the RCP8.5 scenario, most CMIP5 models not only project annual mean increases to tropical temperature and precipitation (Figure 2(a–b)), but also consistent changes to the seasonality of these quantities (Figure 2(c–e)).

Annual mean surface temperature increases throughout the tropics, especially on land, with the greatest ocean warming occurring on or near the equator (Figure 2(a)). Increases in precipitation in the tropical oceans (Figure 2(b)) mainly occur in regions with large climatological precipitation (Held and Soden 2006; Chou and Neelin 2004), as well as regions that have large increases in SST (Xie et al. 2010; Huang et al. 2013).

The amplitude of surface temperature (Figure 2(c)) broadly increases throughout much of the tropics, aside from the Western Pacific. This is in agreement with the tropical-wide amplitude increase of PC1, calculated by performing an EOF analysis over tropical SST (25°S–25°N). Changes in the amplitude of the annual cycle of precipitation, plotted in Figure 2(d), are positive along much of the equator, especially in the Western Pacific and Indian Ocean, where the increase in amplitude is above 50%. These changes share a similar pattern to those of the annual mean SST change in Figure 2(a). Many land monsoon regions also show increases in the amplitude of the annual cycle of precipitation, indicating an increase of summer precipitation relative to winter precipitation (Biasutti and Sobel 2009; Seth et al. 2011; Sobel and Camargo 2011; Seth et al. 2013).

The phase of surface temperature (Figure 2(e)) delays for much of the NH tropical ocean off the equator, as well as in the Eastern Pacific and Indian Ocean in the SH. While there are some regions of phase advance, the PC1 of tropical SST has a weak phase delay. Precipitation (Figure 2(f)) is noisier. Despite phase advances in the tropical Atlantic and Eastern Pacific, PC1 of tropical, oceanic precipitation shows a phase delay.

We demonstrate the scatter between models in Figure 3 which shows the zonal mean seasonality changes over ocean for the individual models and the multi-model mean. Amplitude changes of SST (Figure 3(a)) are more tightly grouped than those of precipitation

(Figure 3(b)), though the changes in precipitation are larger. The same is true for the phase delays (Figures 3(c) and (d)). We have only plotted data for which the annual cycle makes up at least 80% of the total variance.

We summarize the tropical CMIP5 changes in Table 2. All models predict increases in the annual mean of SST and oceanic precipitation with multi-model mean changes of 2.9 K and 0.2 mm day^{-1}, respectively. There is less agreement among models on the sign of the annual mean change in terrestrial precipitation, which has a multi-model mean increase of 0.1 mm day^{-1}. However, the amplitude increase and phase delay of precipitation are more robust over land than ocean – nearly all models agree on the sign of the changes in land precipitation. In the multi-model mean, phase delays are larger over land (3.5 days) than ocean (2.7 days), though the amplitude increases are larger over ocean (15.5%) than land (8.2%). Seasonal changes of SST are weaker than those for precipitation, though most models show an amplitude increase and phase delay.

To investigate the nature of the seasonal precipitation changes in response to greenhouse gases, we perform a moisture budget analysis, following and extending previous work (Chou et al. 2007; Tan et al. 2008; Chou and Lan 2011; Huang et al. 2013). The moisture equation in flux form is

$$\left\langle \vec{\nabla} \cdot (\vec{u}q) \right\rangle = E - P - \left\langle \frac{\partial q}{\partial t} \right\rangle, \tag{1}$$

where $\vec{u}$ is the horizontal velocity, q is the specific humidity multiplied by the latent heat of vaporization, E is the evaporation and P is the precipitation given in units of W m^{-2} (1 mm day^{-1} $\approx$ 28 W m^{-2}). Angle brackets indicate a mass-weighted vertical integration from the surface to the tropopause:

$$\langle A \rangle = \frac{1}{g} \int_{p_{sfc}}^{p_{trop}} A \mathrm{d}p. \tag{2}$$

Assuming that $\omega = 0$ at the surface and the tropopause, then $\left\langle \vec{\nabla} \cdot (\vec{u}q) \right\rangle = \left\langle \omega \frac{\partial q}{\partial p} \right\rangle + \left\langle \vec{u} \cdot \vec{\nabla} q \right\rangle$, and the moisture budget can be written as:

$$P = E + \left\langle -\vec{u} \cdot \vec{\nabla} q \right\rangle + \left\langle -\omega \frac{\partial q}{\partial p} \right\rangle - \left\langle \frac{\partial q}{\partial t} \right\rangle. \tag{3}$$

We apply this to monthly data for the historical simulation for 1980–1999 and confirm that in the annual mean, the dominant balance averaged over the global mean tropics is between P and E with a smaller contribution from $\left\langle -\omega \frac{\partial q}{\partial p} \right\rangle$, which becomes substantial in the deep tropics between 10°S and 10°N (Figure 4(a)). The sum of the budget terms overestimates P by about 15% when averaged over the tropics, but with better agreement in the deep tropics. Sub-monthly transients likely account for most of this difference (Seager and Henderson 2013).

We also calculate the annual cycle of the budget. By zonally averaging each term in Equation 3 and then calculating the Fourier transform, we obtain the amplitude and phase of the first harmonic of each term in Equation 3. We calculate the phase and amplitude for the sum of the terms on the right hand side of the equation since this is not simply the sum of the phases or the sum of the amplitudes of each term. Analyzing the annual cycle of the budget allows us to visualize the annual cycle with two variables (amplitude and phase) rather than 12 monthly values and concisely determine which term balances precipitation on seasonal time scales.

We plot the amplitude of the terms in the moisture budget in Figure 4(b). The amplitude of precipitation is similar in latitudinal structure to the amplitude of the sum of the terms on the right hand side of the budget, but about 15% larger. As was the case for the annual mean, agreement is best in the deep tropics. Because the amplitude of the sum of the terms is very similar to the amplitude of $\left\langle -\omega \frac{\partial q}{\partial p} \right\rangle$, we conclude that the primary balance of A_P is with $A_{\left\langle -\omega \frac{\partial q}{\partial p} \right\rangle}$ – the amplitude of vertical moisture advection. These two terms are also in phase throughout the tropics as demonstrated in Figure 4(c), indicating that the seasonal cycles of P and $\left\langle -\omega \frac{\partial q}{\partial p} \right\rangle$ are in balance. The phases of the budget terms (Figure 4(c)) also shows that ϕ_P is well described by the phase of the sum of the budget terms, except where the amplitude of the annual cycle is nearly zero. For the CMIP5 models this occurs around 2°N and poleward of around 20°N.

We investigate how A_P, ϕ_P, and other terms change in the RCP8.5 scenario by taking the

Fourier transform of Equation 3 and solving for A_P and ϕ_P, while neglecting the moisture storage terms as these are of the same order as the residual of the budget. Assuming that the changes for each term between the RCP8.5 and control simulations (averaged over 2080–2099 and 1980–1999, respectively) are sufficiently small, we can write ΔA_P and $\Delta\phi_P$ as a linear combination of perturbations to the amplitudes and phase of each term in Equation 3 (see Appendix A). The contribution of each perturbation term to either ΔA_P or $\Delta\phi_P$ is the product of the perturbation term and a factor that depends on the relative amplitude and phases of the budget terms.

We plot the contribution from each term in Figure 5(a). The solid, black line is the actual amplitude change in precipitation, and the dashed, black line is the sum of the contributions from the perturbations to each term, which will resemble ΔA_P if our decomposition is accurate. ΔA_P is positive throughout the tropics, and has two maxima: at 7.5°S and 7.5°N, which coincide with the maxima in the climatology. The sum of perturbations matches ΔA_P well between 20°S and 20°N, except just north of the equator, where the annual cycle is weak. The primary contribution to the sum comes from $\Delta A_{\langle -\omega\partial q/\partial p\rangle}$, the changes in the amplitude of the seasonal cycle of vertical moisture advection – unsurprising since this term dominates the budget in the control simulation (Figure 4(b)). Similarly for phase, $\Delta\phi_P$ is well described by the sum of the contributions from the individual terms in the tropics, aside from poleward of 20°N and around 2°N where the climatological annual cycle is weak (Figure 5(b)). There is no single term that primarily contributes to balancing $\Delta\phi_P$, though $\Delta\phi_{\left\langle -\omega\frac{\partial q}{\partial p}\right\rangle}$ provides a substantial contribution.

Because of the strong balance in the annual cycle budget between P and $\left\langle -\omega\frac{\partial q}{\partial p}\right\rangle$, it is unsurprising that the changes in the amplitude of precipitation are balanced by similar changes in $A_{\left\langle -\omega\frac{\partial q}{\partial p}\right\rangle}$. To gain insight into what aspect of $\left\langle -\omega\frac{\partial q}{\partial p}\right\rangle$ is changing in the RCP8.5 simulation we can decompose changes in $A_{\left\langle -\omega\frac{\partial q}{\partial p}\right\rangle}$ and $\phi_{\left\langle -\omega\frac{\partial q}{\partial p}\right\rangle}$ into contributions from six different terms: changes in the annual mean, amplitude, and phase of ω and $\frac{\partial q}{\partial p}$ (See Appendix B for the full procedure).

First we consider the decomposition of $\Delta A_{\left\langle -\omega \frac{\partial q}{\partial p} \right\rangle}$ and plot the results in Figure 5(c). The sum of the decomposition is very similar to $\Delta A_{\left\langle -\omega \frac{\partial q}{\partial p} \right\rangle}$, validating our procedure and neglect of small terms. For most of the tropics, the dominant contribution is from $\frac{\partial \Delta \overline{q}}{\partial p}$ – an increase in the annual mean vertical gradient of water vapor. This effect is a thermodynamic consequence of the 3 K warming. Because the relative humidity stays roughly constant, the rise in mean temperature increases the moisture throughout the troposphere, but especially in the lower atmosphere due to Clausius-Clapeyron. The seasonally varying, ascending branch of the Hadley Cell then converts the enhanced vertical moisture gradient into additional precipitation (Held and Soden 2006). Because the seasonal cycle of vertical motion in the deep tropics is upward in the summer, the increase in $\frac{\partial \Delta \overline{q}}{\partial p}$ results in an increase in A_P.

The other term that significantly affects $\Delta A_{\left\langle -\omega \frac{\partial q}{\partial p} \right\rangle}$ is due to the change in the amplitude of the circulation. This term provides a small positive contribution near the equator, but contributes negatively to A_P for much of the tropics and partially compensates for the increase of $\frac{\partial \Delta \overline{q}}{\partial p}$. The negative contribution is associated with a reduction in the amplitude of the seasonal cycle of vertical motion due to some combination of reduced upward motion in summer and reduced subsidence in winter – indicative of a slowdown in the tropical circulation, a robust feature of the CMIP models (Held and Soden 2006; Vecchi et al. 2006).

Previous studies have found similar results for changes due to increased greenhouse gases in the coupled models (Chou et al. 2007; Tan et al. 2008; Chou and Lan 2011; Huang et al. 2013). In particular, Tan et al. (2008) compared the changes in various terms of the moisture budget in summer and winter months. While they did not decompose changes in $\left\langle -\omega \frac{\partial q}{\partial p} \right\rangle$ into annual mean and seasonal deviations, they found that changes in $\left\langle -\omega \frac{\partial \Delta q}{\partial p} \right\rangle$ drove an increase in summer precipitation in the coupled models with some compensation from $\left\langle -\Delta\omega \frac{\partial q}{\partial p} \right\rangle$. We confirm these results in the CMIP5 models using Fourier methods and extend previous studies by analyzing the phase response.

We decompose $\Delta \phi_{\left\langle -\omega \frac{\partial q}{\partial p} \right\rangle}$ into a linear combination of terms, as we did with amplitude, and plot the results in Figure 5(d). While $\Delta \phi_{\left\langle -\omega \frac{\partial q}{\partial p} \right\rangle}$ is not solely responsible for the changes in $\Delta\phi_P$, it is a major contributor to $\Delta\phi_P$. Between 20°S and 20°N, $\Delta\phi_{\langle -\omega \frac{\partial q}{\partial p} \rangle}$ is mostly positive and balanced by two contributions: a phase delay of ω and to a lesser extent a change in the amplitude of ω. This result rules out thermodynamic causes from the Clausius-Clapeyron relation for causing the phase delay of precipitation and indicates the importance of changes in the timing of circulation, whose causes are not yet known.

4. Uniform Warming Experiment

We first investigate the effects that a spatially uniform, mean temperature increase has on the seasonal characteristics of precipitation by increasing the SST by 3 K (Cess et al. 1990), almost identical to the annual, tropical, multi-model mean SST increase of 2.9 K in the CMIP5 models between the end of the 21st and 20th centuries. As a result of the SST warming, annual mean precipitation increases throughout the tropics.

Using the EOF method to quantify the change in the seasonal characteristics of precipitation, we find an amplification of 22.2% of the seasonal cycle of precipitation when the SST is uniformly increased by 3 K. The UW simulation also has a delayed phase relative to the control simulation of 4.7 days.

To gain a better understanding of why the changes in the seasonality of precipitation are so similar in the UW simulation to those of CMIP5, we repeat our budget analysis for the UW simulation. We begin by comparing the control simulation to that of the historical CMIP5 simulations.

In the annual mean, the various terms of the moisture budget of the control simulation (Figure 6(a)) are similar to those of the CMIP5 models, except many are slightly stronger. There is also a larger interhemispheric asymmetry of precipitation and vertical moisture advection in the AGCM compared to the CMIP5 models, perhaps because of an erroneous, double ITCZ in the coupled models (Lin 2007). The amplitude of the control simulation (Figure 6(b)) is weaker than that for the CMIP5 multi-model mean. Although there are two maxima in the amplitude of precipitation, they are weaker and less well-defined than for the CMIP5 models. For both the annual mean and amplitude as well as for the phase (Figure 6(c), the sum of the decomposition of budget terms describes the precipitation well, including near the equator and poleward of 20°N, where it failed for the CMIP5 models.

Next we turn our attention to changes in the seasonal cycle of precipitation and related budget terms due to a 3 K uniform SST warming. We plot the amplitude change and the contributions to the amplitude change in Figure 7(a). The amplitude of precipitation increases throughout the tropics, and has two maxima, around 2°N and 15°N. This latitudinal structure is roughly similar to those of the CMIP5 models, except the peaks are displaced, weaker and broader than those of the CMIP5 models. The sum of budget terms, dominated by $\Delta A_{\langle -\omega \frac{\partial q}{\partial p} \rangle}$, agrees with A_P, but greatly exaggerates the maxima for reasons that are unclear.

The phase changes of precipitation agree well with the sum of the contributions (Figure 7(b)) and show a delay at the equator and poleward of 12° in both hemispheres with advances around 5°N and 5°S. This latitudinal structure is quite similar to that of the coupled models (compare to Figure 5(b)). But unlike in the coupled models, there is one term that mainly balances $\Delta\phi_P - \Delta\phi_{\langle -\omega \frac{\partial q}{\partial p} \rangle}$.

Next we decompose the changes in $\Delta A_{\langle -\omega \frac{\partial q}{\partial p} \rangle}$, since this is the primary balance with ΔA_P (Figure 7(c)). As with the RCP8.5 CMIP5 models, the primary balance is with $\partial \Delta \overline{q}/\partial p$. The annual mean increase in moisture gradient contributes to the seasonal amplification of precipitation in the same way as in the coupled models. Unlike in the RCP8.5 case, though, the latitudinal structure of these changes is not as symmetric about the equator and has broader peaks. Similarly, a decrease in the amplitude of the circulation compensates for some of the increase in $\partial \Delta \overline{q}/\partial p$, but with a weaker and less symmetrical latitudinal structure about the equator than in the RCP8.5 case.

Returning to the budget for the phase changes, we decompose $\Delta\phi_{\langle -\omega \frac{\partial q}{\partial p} \rangle}$ into a linear combination of terms, as we did with amplitude and plot the results in Figure 7(d). Here the decomposition works very well as the linear combination of decomposed terms is nearly identical to $\Delta\phi_{\langle -\omega \frac{\partial q}{\partial p} \rangle}$. The dominant terms are due to circulation – changes in both the phase and amplitude of ω contribute to $\Delta\phi_{\langle -\omega \frac{\partial q}{\partial p} \rangle}$, with a larger contribution from $\Delta\phi_\omega$. These changes are similar to those in the RCP8.5 models, though in that simulation $\Delta\phi_{\langle -\omega \frac{\partial q}{\partial p} \rangle}$ was not the sole, dominant contributor to $\Delta\phi_P$.

Despite the differences between coupled models with realistic 21st century forcings including greenhouse gas changes and aerosols and an AGCM with a uniform SST increase, there is much similarity in their seasonal precipitation responses. Both show an amplification and phase delay in the seasonal cycle of precipitation in the tropics with similar latitudinal structure. Moreover, the terms that contribute to these seasonal changes are very similar between these simulations, indicating that the same processes may be operating between models.

5. Modified Seasonality Experiment

In the second set of experiments, we investigate the effect that changing only the seasonal characteristics of SST has on the seasonal cycle of precipitation. We run seven simulations with amplitude as in the control run and phase shifts varying from a 15 day advance to a 15 day delay and plot the resulting changes in the phase of precipitation as black circles in Figure 8(a). The results show that a delayed SST causes delayed precipitation and advanced SST causes advanced precipitation. Moreover, the relationship between the phases of SST and precipitation is linear. This is the case even when the amplitude of the annual cycle of SST is perturbed as well.

For all sets of simulations with identical changes in the amplitude of SST, the change in the phase of precipitation is weaker than the imposed change in the phase of SST (the slope of the linear relationship is less than one). This low sensitivity appears to be due to land. The phase of precipitation in Figure 8(a) is calculated from a PC associated with an

EOF structure that includes both land and ocean (Figure 1). If we perform an EOF analysis limited to oceanic precipitation and calculate the seasonality of precipitation from its PC, the slope is nearly one, as in Figure 8(b). Likewise, when we limit our EOF analysis to precipitation over land (Figure 8(c)) we find a slope that is close to zero. This is consistent with Biasutti et al. (2003) and Biasutti et al. (2004), who found that the seasonality of precipitation over ocean is primarily due to the effects of SST in an AGCM, while over land it is primarily due to insolation directly.

As was the case for phase, the change in amplitude of the annual cycle of precipitation is linearly related with a positive slope to the change in amplitude of the annual cycle of SST. Figure 8(d) shows the relationship holds for any set of simulations with the same phase of SST and varying amplitudes of SST, though again, the slope is less than one. In this case, limiting the EOF to ocean (Figure 8(e)) results in a slightly stronger sensitivity, but with a slope still less than one. We would expect a sensitivity of one if the relationship between SST and tropical, oceanic precipitation were linear. In reality and in GCMs, the relationship between SST and precipitation is more complicated, as precipitation is suppressed in a convectively stable environment.

When we constrain the EOF to land (Figure 8(f)), the slope is still greater than zero, but very small. Part of the reason for the shallow slope is because precipitation is positive definite. Near zero winter precipitation is the case in many land-monsoon regions, such as the Sahel, South Asia, Australia, and South Africa. In these regions, even a 10% increase in the amplitude of the annual cycle of precipitation would cause winter precipitation to become negative in the AGCM.

In addition to the direct forcing of phase on phase and amplitude on amplitude, there are cross-effects: the phase of SST affects the amplitude of precipitation and the amplitude of SST changes the phase of precipitation, as illustrated by the spread of the colored markers in Figure 8. If we limit the EOF analysis to oceanic precipitation only (Figure 8(b) and (e)), the effect remains with about the same magnitude as for the case with global precipitation

(Figure 8(a) and (d)). The effect is not an artifact of EOF analysis - it also exists when we perform our analysis with a Fourier transform of the data. If oceanic, tropical precipitation were entirely dependent on SST alone, we would not expect these cross-effects.

We interpret these effects as primarily due to the presence of land. Limiting the EOF to ocean doesn't eliminate the cross-effects because tropical convection can organize on large scales that cover both ocean and land for phenomena like monsoons, inextricably linking the two domains. In this sense, oceanic precipitation is a function of both SST and insolation, which peaks earlier in the year.

The cross-effects can be understood mathematically by thinking of tropical precipitation P as a linear combination of insolation (I) and SST (T): $P = \sigma I + \tau T$, where σ and τ give the relative strengths of I and T and ensure correct units. By writing this equation in seasonal form as $A_P e^{-i\phi_P} = \sigma A_I + \tau A_T e^{-i\phi_T}$ (where A and ϕ are the amplitude and phase lag from insolation of the annual cycle for the subscripted quantities) and solving for the seasonality of precipitation we find:

$$A_P = \sqrt{\sigma^2 A_I^2 + \tau^2 A_T^2 + 2\sigma\tau A_I A_T \cos\phi_T)} \tag{4}$$

$$\phi_P = \arctan\left(\frac{\tau A_T \sin\phi_T}{\tau A_T \cos\phi_T + \sigma A_I}\right). \tag{5}$$

Assuming small changes to the phase and amplitude of SST, we can write the resulting changes to the phase and amplitude of precipitation as:

$$\Delta A_P = \Delta A_T \left(\frac{\tau^2 A_T + \tau\sigma A_I \cos\phi_T}{A_P}\right) + \Delta\phi_T \left(\frac{-\tau\sigma A_I A_T \sin\phi_T}{A_P}\right) \tag{6}$$

$$\Delta\phi_P = \Delta A_T \left(\frac{\tau\sigma A_I \sin\phi_T}{A_P^2}\right) + \Delta\phi_T \left(\frac{\tau\sigma A_I A_T \cos\phi_T + \tau^2 A_T^2}{A_P^2}\right). \tag{7}$$

Since all of the amplitudes and phases are positive and $\phi_T \approx 73$ days for tropically averaged SST, this model gives the expected result that delayed and amplified SST produces delayed and amplified precipitation. The model also predicts the presence of cross-effects with the right sign: a delayed SST leads to a weakened seasonal cycle of precipitation and an amplified SST leads to a delayed seasonal cycle of precipitation. The magnitude of these effects depend not only on the various unforced amplitudes and phases, but also on the relative importance of SST and insolation at forcing precipitation.

We also confirm that this is the case by running aquaplanet simulations, which have no land – only an ocean with an imposed seasonally varying SST – and no zonal asymmetries in the boundary conditions. As expected, in the aquaplanet simulations the direct effects are still present: delayed and amplified SST yields delayed and amplified precipitation, respectively. However, the cross-effects are smaller and no longer statistically significant at the 95% level. The effect that the amplitude of SST has on the phase of precipitation is reduced by 60% in the aquaplanet simulations and the effect that the phase of SST has on the amplitude of precipitation is reduced by 85%. Insolation still varies throughout the year, and has a phase-locked seasonal cycle of shortwave absorption in the atmosphere that may account for the remainder of the cross-effects. But when the effects of land and other zonal asymmetries are totally removed, the cross-effects diminish considerably.

We also repeat the budget analysis that we performed for the CMIP5 and UW simulations for a simulation with a 5-day SST phase delay and a 10% SST amplitude increase (p5a10) and plot the results in Figure 9. The chosen values of phase delay and amplitude increase to SST are exaggerated compared to the CMIP5 multi-model mean in order to obtain clearer results. In this simulation ΔA_P has a similar latitudinal structure to both the RCP8.5 and UW simulations and increases the most around 10°N and 10°S – slightly more widely separated than in either simulation. The sum of the contributions generally agrees with the actual change in ΔA_P, but overestimates the changes near the peaks (though overall the amplitude changes are weaker than the other simulations by a factor of 2–3). As in the other simulations, the primary contribution comes from $\Delta A_{\langle -\omega \frac{\partial q}{\partial p} \rangle}$. $\Delta \phi_P$ is positive throughout the tropics, with twin peaks near the equator – a different latitudinal structure than for RCP8.5 or UW. But like the UW simulation, it is balanced by $\Delta \phi_{\langle -\omega \frac{\partial q}{\partial p} \rangle}$ (Figure 9(b)).

When we decompose the changes to $\Delta A_{\left\langle -\omega\frac{\partial q}{\partial p}\right\rangle}$ (Figure 9(c)), we find that the most substantial contribution arises from a change in the amplitude of the circulation with a supporting contribution from a change in the phase of the circulation. In the RCP8.5 and UW simulations, by comparison, most of the change was due to the annual mean increase in moisture gradient, $\frac{\partial \Delta \overline{q}}{\partial p}$ with a negative contribution from a change in the amplitude of circulation. Phase changes in $\left\langle -\omega\frac{\partial q}{\partial p}\right\rangle$ (Figure 9(d)), are also balanced by changes in the circulation - in this case mostly from a change in the phase of the circulation and some from a change in the amplitude of ω. In this simulation, moisture changes are unimportant for understanding the changes in the seasonality of precipitation. Instead the seasonality changes of SST are communicated to the precipitation via the circulation.

6. Comparison Between AGCM Experiments and CMIP5

To better understand the nature of the seasonal changes in precipitation in the CMIP5 models, we construct an empirical model from the results of our AGCM simulations. For example, since the CMIP5 multi-model mean and the UW simulation both have almost identical mean temperature increases in the tropical average (2.9 K for CMIP5 and 3 K for the UW simulation), we can construct the amplitude and phase change in precipitation in the CMIP5 due to annual mean warming from the results of the UW simulation. Because we know the amplitude change of temperature in the CMIP5 models and the sensitivity of amplitude changes of precipitation to amplitude changes of temperature (the slope of the black dots in Figure 8(a)), their product is the change of the amplitude of precipitation in the CMIP5 models due to ΔA_T. Similarly, we can repeat this for phase as well as for the cross-effects (the effect of $\Delta \phi_T$ on ΔA_P and ΔA_T on $\Delta \phi_P$).

There are some significant caveats to this method. First and foremost, we are assuming that changes in SST are driving all of the seasonality changes in precipitation. In reality there may be other effects which we've ignored. Second, we are using a model without an interactive ocean to infer results from models with interactive oceans. Among other things, this ignores any possibility of changes in the seasonality of precipitation feeding back on the seasonality of SST. It is possible that changes in the seasonality of SST are a consequence of changes in the seasonality of precipitation and not the other way around in the CMIP5 models. Finally, we are not simulating the actual spatial pattern of annual mean or annual cycle changes of SST in our AGCM. Instead we simulate a uniform change across the tropical oceans and calculate the results for the tropics as a whole.

We list the results in Table 3 for both ocean and land. For ocean, over 90% of the contribution to A_P comes from the annual mean increase of SST, with around 10% from the increase in A_T and a small negative contribution due to the cross-effect of ϕ_T. As a whole, these contributions outweigh the actual measured increase in A_P by 60%. Similarly, for ϕ_P the largest contribution (4.7 days) is from the annual mean SST increase, while A_T contributes 1.4 days and ϕ_T contributes only 1.1 days. While $\partial\phi_P/\partial\phi_T \approx 1$, $\Delta\phi_{T,CMIP5}$ is only 1.1 days. Again the total changes constructed by this empirical model are larger than the actual CMIP5 changes, here by over a factor of 2.

Over land the results are similar, though each term is proportionally smaller than over ocean. As a result the sum of the inferred changes for A_P is 8.1%, almost identical to the actual value for CMIP5 of 8.2%. For ϕ_P, the sum of the contributions actually underestimates the total by 17%. The better agreement over land compared to ocean suggests that coupling to a thermodynamically interactive lower boundary may be important. In our simulations, the land temperature is interactive, satisfying a consistent surface energy budget, while the ocean temperature is not. It is plausible that under some circumstances, an interactive ocean mixed layer could respond locally to large-scale atmospheric influences in such a way as to mute or otherwise substantially alter the precipitation response compared to what would occur over an ocean surface with fixed SST (e.g., Chiang and Sobel (2002); Wu and Kirtman (2005, 2007); Emanuel and Sobel (2013)).

While much of this study has focused on precipitation changes over ocean, we now consider how the seasonality changes manifest over land. Previous work has identified a phase delay and amplitude increase in the coupled models in land monsoon regions (Biasutti and Sobel 2009; Seth et al. 2011, 2013). While not specifically confined to monsoon regions, Table 2 indicates that the delays in the phase of precipitation are not only larger over tropical land but also more robust than over tropical ocean – 34 of the 35 models project a phase delay over tropical land.

Our forced simulations produce similar changes in land monsoon regions to those of CMIP5. Specifically the UW simulation and the p5a10 simulation each show an amplification and phase delay in the annual cycle of precipitation in NH land monsoon regions, defined by averaging over land and over longitudes as defined in Seth et al. (2011).

Figure 10(a) and (b) illustrate this for the UW simulation with climatological precipitation (contour lines) and the percentage change in precipitation (shading) for NH and SH monsoon regions, respectively. In both hemispheres the peak rainy season gets wetter, amplifying the seasonal cycle of precipitation. Additionally, an early season deficit and a late season excess of rain produce a phase delay. For the p5a10 simulation (Figure 10(c) and (d)), the amplitude increase is milder than in the UW simulation, but the phase delay is of similar strength.

The structures of the changes in both simulations bear much similarity, especially at the beginning and the end of the monsoon season, despite the different nature of the imposed changes in SST between simulations. But perhaps this should not be entirely surprising given the contributions to phase changes of precipitation in the budget analysis. As illustrated in Figures 7(d) and 9(d), the leading contribution to phase changes in precipitation in the tropics are changes in the seasonal cycle of ω. Both simulations show similar changes in the phase of precipitation and the phase of the atmospheric circulation, especially between 15°–25° in both hemispheres. In both cases the timing of the atmospheric circulation is playing an important role, perhaps because of the important role of circulation in monsoon regions in influencing precipitation (Trenberth et al. 2000).

7. Conclusions

We have studied the annual mean and seasonal response of tropical surface temperature and precipitation in the CMIP5 models to additional radiative forcing specified by the RCP8.5 scenario. We found, in addition to annual mean increases of SST and oceanic precipitation, and consistent with past studies, that the amplitude of the seasonal cycles of SST and oceanic precipitation increased by 4.2% and 15.5% and that the phase was delayed by 1.1 days and 2.7 days, respectively.

To better understand these results, we performed simulations with an AGCM in which we measured the precipitation response to changes in the annual mean and seasonal cycle of SST. Increasing the annual mean SST everywhere by 3 K in the UW simulation caused not only an increase in annual mean tropical precipitation, but also an amplification and a phase delay of precipitation. We obtained seasonal precipitation changes of the same sign, albeit smaller, from the p5a10 simulation in which we left the mean value of SST unchanged, but amplified SST by 10% and delayed it by 5 days. In terms of the magnitude of the seasonal precipitation changes, the CMIP5 results are much more similar to the UW simulation than to the p5a10 simulation.

Further support for the similarity between the CMIP5 models and the UW simulations comes from studying the annual cycle of the moisture budget. From an analysis of the CMIP5 moisture budget we corroborate the work of previous studies (Tan et al. 2008; Huang et al. 2013) that found that the coupled model response of the amplitude of P is consistent with an increase in the annual mean vertical moisture gradient due to the Clausius-Clapeyron relation. This additional boundary layer moisture is vertically advected in the summer months by the ascending branch of the Hadley Cell, while in winter the descending branch of the circulation does not convect this additional moisture. There is also a negative contribution to the amplitude of precipitation from a decrease in the amplitude of the seasonal cycle of vertical motion, consistent with a weakening of tropical circulation. We also find that changes in the phase of precipitation have a more complex balance than the amplitude changes, and are largely balanced by changes in the phase and amplitude of the circulation.

These changes are better reproduced in the UW simulation than in the p5a10 simulation. A uniform SST warming produces amplitude changes in precipitation that are primarily balanced by an increase in the annual mean vertical gradient of moisture, just as in the coupled models. The p5a10 simulation produces a weaker amplification of precipitation compared to the CMIP5 models, despite being forced with exaggerated seasonality changes of SST. Both UW and RCP8.5 also have a weakened seasonal cycle of circulation, which contributes negatively to the changes in precipitation amplitude; p5a10 has an enhanced circulation. In terms of changes in the phase of the annual cycle of precipitation, RCP8.5 is again more similar to UW than to p5a10. While all three simulations have large contributions to changes in the phase of precipitation from changes in both the phase and amplitude of circulation, UW captures the latitudinal structure more accurately.

Because so many of the models have an amplification and delay in the annual cycle of precipitation, the mechanism responsible for this behavior is likely simple. We find that we can reproduce the changes in an AGCM by simply uniformly increasing the SST, further suggesting that this is a robust climate response. The amplitude response can be explained by well-studied mechanisms: the increase in annual mean, vertical moisture gradient due to Clausius-Clapeyron and the slowdown in the circulation (Held and Soden 2006) (though here the slowdown is in the annual cycle). The phase response of precipitation is more complicated, but appears to be, at least in part, due to a phase delay in the circulation. What forces this response is an open question.

The simulations in which we varied the phase and amplitude of SST demonstrated that seasonal changes to SST force seasonal changes in tropical precipitation of the same sign, i.e., delayed SST causes delayed precipitation and amplified SST causes amplified precipitation. These changes are communicated effectively by seasonal changes to the tropical circulation. These effects are not limited to ocean, either. Land monsoon regions are sensitive to the seasonal characteristics of SST in the same way as the ocean. Land is also responsible for cross-effects: changes to the phase of SST affect the amplitude of precipitation and changes to the amplitude of SST affect the phase of precipitation.

These AGCM simulations help inform our understanding of the nature of the seasonal changes in the GCMs. Taking the AGCM results at face value and ignoring any effects from ocean feedbacks or the spatial pattern of changes indicates that over ocean 90% of the amplitude increase and 60% of the phase delay in precipitation is due to the annual mean increase in SST, with the remainder being due to the amplitude increase and phase delay in SST (results are similar for land precipitation). Of course, these simulations do not rule out other potential mechanisms for generating a change in the seasonality of precipitation. Furthermore, it is beyond the scope of this study to determine the cause of the changes to the seasonality of SST in the CMIP5 ensemble due to the inherent limitations of AGCM studies. This means that we cannot rule out the possibility that changes in precipitation are driving changes in SST or that there are feedbacks involved in the coupled models. Despite these limitations, this study demonstrates a feasible way in which the changes in the seasonality of precipitation may arise.

Acknowledgments.

This research was supported by NSF Grant AGS-0946849 and NASA Earth and Space Science Fellowship NNX11AL88H. We thank Gus Correa for providing computer support for the simulations and Naomi Henderson and Haibo Liu for helping with the CMIP3 and CMIP5 datasets. We also wish to thank NCAR for allowing for public use of their GCM. We acknowledge the World Climate Research Programme's Working Group on Coupled Modelling, which is responsible for CMIP, and we thank the climate modeling groups (listed in Table 1 of this paper) for producing and making available their model output. For CMIP the U.S. Department of Energy's Program for Climate Model Diagnosis and Intercomparison provides coordinating support and led development of software infrastructure in partnership with the Global Organization for Earth System Science Portals.

APPENDIX A

Decomposition of Changes to the Moisture Budget

In this section we detail the procedure for expanding changes in the amplitude or phase of precipitation in terms of the amplitude or phase of evaporation, horizontal moisture advection, and vertical moisture advection. We begin by taking the Fourier transform of Equation 3 and neglecting the moisture storage term.

$$A_P e^{-i\phi_P} = A_E e^{-i\phi_E} + A_{\left\langle -\vec{u}\cdot\vec{\nabla}q \right\rangle} e^{-i\phi_{\left\langle -\vec{u}\cdot\vec{\nabla}q \right\rangle}} + A_{\left\langle -\omega\frac{\partial q}{\partial p} \right\rangle} e^{-i\phi_{\left\langle -\omega\frac{\partial q}{\partial p} \right\rangle}} \tag{A1}$$

Solving this equation for the amplitude and phase of precipitation gives

$$\begin{aligned} A_P^2 =& A_E^2 + A^2_{\left\langle -\vec{u}\cdot\vec{\nabla}q \right\rangle} + A^2_{\left\langle -\omega\frac{\partial q}{\partial p} \right\rangle} + 2A_E A_{\left\langle -\vec{u}\cdot\vec{\nabla}q \right\rangle} \cos\left(\phi_E - \phi_{\left\langle -\vec{u}\cdot\vec{\nabla}q \right\rangle}\right) \\ &+ 2A_E A_{\left\langle -\omega\frac{\partial q}{\partial p} \right\rangle} \cos\left(\phi_E - \phi_{\left\langle -\omega\frac{\partial q}{\partial p} \right\rangle}\right) + 2A_{\left\langle -\vec{u}\cdot\vec{\nabla}q \right\rangle} A_{\left\langle -\omega\frac{\partial q}{\partial p} \right\rangle} \cos\left(\phi_{\left\langle -\vec{u}\cdot\vec{\nabla}q \right\rangle} - \phi_{\left\langle -\omega\frac{\partial q}{\partial p} \right\rangle}\right) \end{aligned} \tag{A2}$$

$$\tan\phi_P = \frac{A_E \sin\phi_E + A_{\left\langle -\vec{u}\cdot\vec{\nabla}q \right\rangle} \sin\phi_{\left\langle -\vec{u}\cdot\vec{\nabla}q \right\rangle} + A_{\left\langle -\omega\frac{\partial q}{\partial p} \right\rangle} \sin\phi_{\left\langle -\omega\frac{\partial q}{\partial p} \right\rangle}}{A_E \cos\phi_E + A_{\left\langle -\vec{u}\cdot\vec{\nabla}q \right\rangle} \cos\phi_{\left\langle -\vec{u}\cdot\vec{\nabla}q \right\rangle} + A_{\left\langle -\omega\frac{\partial q}{\partial p} \right\rangle} \cos\phi_{\left\langle -\omega\frac{\partial q}{\partial p} \right\rangle}}. \tag{A3}$$

Applying a small perturbation to Equations A2 and A3 and neglecting 2nd order terms results in a linear combination of perturbations to the phases and amplitudes of the budget terms.

$$\Delta A_P = \frac{1}{A_P} \times \tag{A4}$$

$$\begin{bmatrix} A_E + A_{\langle -\vec{u}\cdot\vec{\nabla}q\rangle} \cos\left(\phi_E - \phi_{\langle -\vec{u}\cdot\vec{\nabla}q\rangle}\right) + A_{\langle -\omega\frac{\partial q}{\partial p}\rangle} \cos\left(\phi_E - \phi_{\langle -\omega\frac{\partial q}{\partial p}\rangle}\right) \\ A_{\langle -\vec{u}\cdot\vec{\nabla}q\rangle} + A_E \cos\left(\phi_{\langle -\vec{u}\cdot\vec{\nabla}q\rangle} - \phi_E\right) + A_{\langle -\omega\frac{\partial q}{\partial p}\rangle} \cos\left(\phi_{\langle -\vec{u}\cdot\vec{\nabla}q\rangle} - \phi_{\langle -\omega\frac{\partial q}{\partial p}\rangle}\right) \\ A_{\langle -\omega\frac{\partial q}{\partial p}\rangle} + A_E \cos\left(\phi_{\langle -\omega\frac{\partial q}{\partial p}\rangle} - \phi_E\right) + A_{\langle -\vec{u}\cdot\vec{\nabla}q\rangle} \cos\left(\phi_{\langle -\omega\frac{\partial q}{\partial p}\rangle} - \phi_{\langle -\vec{u}\cdot\vec{\nabla}q\rangle}\right) \\ -A_E A_{\langle -\vec{u}\cdot\vec{\nabla}q\rangle} \sin\left(\phi_E - \phi_{\langle -\vec{u}\cdot\vec{\nabla}q\rangle}\right) - A_E A_{\langle -\omega\frac{\partial q}{\partial p}\rangle} \sin\left(\phi_E - \phi_{\langle -\omega\frac{\partial q}{\partial p}\rangle}\right) \\ -A_{\langle -\vec{u}\cdot\vec{\nabla}q\rangle} A_E \sin\left(\phi_{\langle -\vec{u}\cdot\vec{\nabla}q\rangle} - \phi_E\right) - A_{\langle -\vec{u}\cdot\vec{\nabla}q\rangle} A_{\langle -\omega\frac{\partial q}{\partial p}\rangle} \sin\left(\phi_{\langle -\vec{u}\cdot\vec{\nabla}q\rangle} - \phi_{\langle -\omega\frac{\partial q}{\partial p}\rangle}\right) \\ -A_{\langle -\omega\frac{\partial q}{\partial p}\rangle} A_E \sin\left(\phi_{\langle -\omega\frac{\partial q}{\partial p}\rangle} - \phi_E\right) - A_{\langle -\omega\frac{\partial q}{\partial p}\rangle} A_{\langle -\vec{u}\cdot\vec{\nabla}q\rangle} \sin\left(\phi_{\langle -\omega\frac{\partial q}{\partial p}\rangle} - \phi_{\langle -\vec{u}\cdot\vec{\nabla}q\rangle}\right) \end{bmatrix}^{\top} \begin{bmatrix} \Delta A_E \\ \Delta A_{\langle -\vec{u}\cdot\vec{\nabla}q\rangle} \\ \Delta A_{\langle -\omega\frac{\partial q}{\partial p}\rangle} \\ \Delta\phi_E \\ \Delta\phi_{\langle -\vec{u}\cdot\vec{\nabla}q\rangle} \\ \Delta\phi_{\langle -\omega\frac{\partial q}{\partial p}\rangle} \end{bmatrix}$$

$$\Delta\phi_P = \frac{\cos^2\phi_P}{\left(A_E\cos\phi_E + A_{\langle -\vec{u}\cdot\vec{\nabla}q\rangle}\cos\phi_{\langle -\vec{u}\cdot\vec{\nabla}q\rangle} + A_{\langle -\omega\frac{\partial q}{\partial p}\rangle}\cos\phi_{\langle -\omega\frac{\partial q}{\partial p}\rangle}\right)^2} \times \tag{A5}$$

$$\begin{bmatrix} A_{\langle -\vec{u}\cdot\vec{\nabla}q\rangle} \sin\left(\phi_E - \phi_{\langle -\vec{u}\cdot\vec{\nabla}q\rangle}\right) + A_{\langle -\omega\frac{\partial q}{\partial p}\rangle} \sin\left(\phi_E - \phi_{\langle -\omega\frac{\partial q}{\partial p}\rangle}\right) \\ A_E \sin\left(\phi_{\langle -\vec{u}\cdot\vec{\nabla}q\rangle} - \phi_E\right) + A_{\langle -\omega\frac{\partial q}{\partial p}\rangle} \sin\left(\phi_{\langle -\vec{u}\cdot\vec{\nabla}q\rangle} - \phi_{\langle -\omega\frac{\partial q}{\partial p}\rangle}\right) \\ A_E \sin\left(\phi_{\langle -\omega\frac{\partial q}{\partial p}\rangle} - \phi_E\right) + A_{\langle -\vec{u}\cdot\vec{\nabla}q\rangle} \sin\left(\phi_{\langle -\omega\frac{\partial q}{\partial p}\rangle} - \phi_{\langle -\vec{u}\cdot\vec{\nabla}q\rangle}\right) \\ A_E^2 + A_E A_{\langle -\vec{u}\cdot\vec{\nabla}q\rangle} \cos\left(\phi_E - \phi_{\langle -\vec{u}\cdot\vec{\nabla}q\rangle}\right) + A_E A_{\langle -\omega\frac{\partial q}{\partial p}\rangle} \cos\left(\phi_E - \phi_{\langle -\omega\frac{\partial q}{\partial p}\rangle}\right) \\ A_{\langle -\vec{u}\cdot\vec{\nabla}q\rangle}^2 + A_{\langle -\vec{u}\cdot\vec{\nabla}q\rangle} A_E \cos\left(\phi_{\langle -\vec{u}\cdot\vec{\nabla}q\rangle} - \phi_E\right) + A_{\langle -\vec{u}\cdot\vec{\nabla}q\rangle} A_{\langle -\omega\frac{\partial q}{\partial p}\rangle} \cos\left(\phi_{\langle -\vec{u}\cdot\vec{\nabla}q\rangle} - \phi_{\langle -\omega\frac{\partial q}{\partial p}\rangle}\right) \\ A_{\langle -\omega\frac{\partial q}{\partial p}\rangle}^2 + A_{\langle -\omega\frac{\partial q}{\partial p}\rangle} A_E \cos\left(\phi_{\langle -\omega\frac{\partial q}{\partial p}\rangle} - \phi_E\right) + A_{\langle -\omega\frac{\partial q}{\partial p}\rangle} A_{\langle -\vec{u}\cdot\vec{\nabla}q\rangle} \cos\left(\phi_{\langle -\omega\frac{\partial q}{\partial p}\rangle} - \phi_{\langle -\vec{u}\cdot\vec{\nabla}q\rangle}\right) \end{bmatrix}^{\top} \times$$

$$\begin{bmatrix} \Delta A_E \\ \Delta A_{\langle -\vec{u}\cdot\vec{\nabla}q\rangle} \\ \Delta A_{\langle -\omega\frac{\partial q}{\partial p}\rangle} \\ \Delta\phi_E \\ \Delta\phi_{\langle -\vec{u}\cdot\vec{\nabla}q\rangle} \\ \Delta\phi_{\langle -\omega\frac{\partial q}{\partial p}\rangle} \end{bmatrix}$$

APPENDIX B

Decomposition the Vertical Moisture Advection Term

Below we decompose $A_{\left\langle -\omega \frac{\partial q}{\partial p} \right\rangle}$ and $\phi_{\left\langle -\omega \frac{\partial q}{\partial p} \right\rangle}$ into changes in the annual mean, amplitude, and phase of ω and $\frac{\partial q}{\partial p}$. We begin by separating the annual mean and deviations from the annual mean

$$\left\langle \omega \frac{\partial q}{\partial p} \right\rangle = \left\langle (\overline{\omega} + \omega') \left(\frac{\partial \overline{q}}{\partial p} + \frac{\partial q'}{\partial p} \right) \right\rangle, \tag{B1}$$

where the overline indicates an annual mean and the prime indicates a deviation from the annual mean. We expand around small changes to this expression

$$\Delta \left\langle \omega \frac{\partial q}{\partial p} \right\rangle = \left\langle \Delta\overline{\omega} \frac{\partial \overline{q}}{\partial p} + \overline{\omega} \frac{\partial \Delta\overline{q}}{\partial p} + \Delta\overline{\omega} \frac{\partial q'}{\partial p} + \overline{\omega} \frac{\partial \Delta q'}{\partial p} + \Delta\omega' \frac{\partial \overline{q}}{\partial p} + \omega' \frac{\partial \Delta\overline{q}}{\partial p} + \Delta\omega' \frac{\partial q'}{\partial p} + \omega' \frac{\partial \Delta q'}{\partial p} \right\rangle, \tag{B2}$$

where we have neglected second order terms, an assumption that we will show is valid momentarily. Next we take the Fourier transform of this equation, as indicated by curly braces:

$$\left\{ \Delta \left\langle \omega \frac{\partial q}{\partial p} \right\rangle \right\} = \left\langle \Delta\overline{\omega} \frac{\partial \{q'\}}{\partial p} \right\rangle + \left\langle \overline{\omega} \frac{\partial \{\Delta q'\}}{\partial p} \right\rangle + \left\langle \{\Delta\omega'\} \frac{\partial \overline{q}}{\partial p} \right\rangle + \left\langle \{\omega'\} \frac{\partial \Delta\overline{q}}{\partial p} \right\rangle. \tag{B3}$$

We have neglected the first two and last two terms of Equation B2, the former because the annual mean doesn't project onto the annual cycle, and the latter because the product of the two terms, each of which has its maximal variance at the annual harmonic, has its maximum variance at the semi-annual harmonic. To determine the exact contribution of the phases and amplitudes of the terms in Equation B3 we perform a similar procedure as before to decompose the effects as a linear combination of perturbation terms. By taking the Fourier

Transform of Equation B3, we obtain

$$\left(\Delta A_{\left\langle -\omega\frac{\partial q}{\partial p}\right\rangle} - iA_{\left\langle -\omega\frac{\partial q}{\partial p}\right\rangle}\Delta\phi_{\left\langle -\omega\frac{\partial q}{\partial p}\right\rangle}\right)e^{-i\phi_{\left\langle -\omega\frac{\partial q}{\partial p}\right\rangle}} = \tag{B4}$$
$$\left(\Delta A_{\left\langle -\Delta\overline{\omega}\frac{\partial\{q'\}}{\partial p}\right\rangle} - iA_{\left\langle -\Delta\overline{\omega}\frac{\partial\{q'\}}{\partial p}\right\rangle}\Delta\phi_{\left\langle -\Delta\overline{\omega}\frac{\partial\{q'\}}{\partial p}\right\rangle}\right)e^{-i\phi_{\left\langle -\Delta\overline{\omega}\frac{\partial\{q'\}}{\partial p}\right\rangle}}$$
$$+\left(\Delta A_{\left\langle -\overline{\omega}\frac{\partial\{\Delta q'\}}{\partial p}\right\rangle} - iA_{\left\langle -\overline{\omega}\frac{\partial\{\Delta q'\}}{\partial p}\right\rangle}\Delta\phi_{\left\langle -\overline{\omega}\frac{\partial\{\Delta q'\}}{\partial p}\right\rangle}\right)e^{-i\phi_{\left\langle -\overline{\omega}\frac{\partial\{\Delta q'\}}{\partial p}\right\rangle}}$$
$$+\left(\Delta A_{\left\langle -\{\Delta\omega'\}\frac{\partial\overline{q}}{\partial p}\right\rangle} - iA_{\left\langle -\{\Delta\omega'\}\frac{\partial\overline{q}}{\partial p}\right\rangle}\Delta\phi_{\left\langle -\{\Delta\omega'\}\frac{\partial\overline{q}}{\partial p}\right\rangle}\right)e^{-i\phi_{\left\langle -\{\Delta\omega'\}\frac{\partial\overline{q}}{\partial p}\right\rangle}}$$
$$+\left(\Delta A_{\left\langle -\{\omega'\}\frac{\partial\Delta\overline{q}}{\partial p}\right\rangle} - iA_{\left\langle -\{\omega'\}\frac{\partial\Delta\overline{q}}{\partial p}\right\rangle}\Delta\phi_{\left\langle -\{\omega'\}\frac{\partial\Delta\overline{q}}{\partial p}\right\rangle}\right)e^{-i\phi_{\left\langle -\{\omega'\}\frac{\partial\Delta\overline{q}}{\partial p}\right\rangle}}$$

Where, for example, $\Delta A_{\left\langle -\Delta\overline{\omega}\frac{\partial\{q'\}}{\partial p}\right\rangle}$ represents the change in amplitude of $\left\langle -\Delta\overline{\omega}\frac{\partial\{q'\}}{\partial p}\right\rangle$ due to a change in the annual mean of ω. Because $\Delta\overline{\omega}$ in $\left\langle -\Delta\overline{\omega}\frac{\partial\{q'\}}{\partial p}\right\rangle$ is multiplied by the vertical moisture gradient at each level and vertically integrated, changes in $\overline{\omega}$ can alter the amplitude or phase of $\left\langle -\Delta\overline{\omega}\frac{\partial\{q'\}}{\partial p}\right\rangle$.

Solving Equation B4 for $\Delta A_{\left\langle -\omega\frac{\partial q}{\partial p}\right\rangle}$ and $\Delta\phi_{\left\langle -\omega\frac{\partial q}{\partial p}\right\rangle}$ separately yields the following.

$$\Delta A_{\left\langle -\omega\frac{\partial q}{\partial p}\right\rangle} = \begin{bmatrix} \cos\left(\phi_{\left\langle -\omega\frac{\partial q}{\partial p}\right\rangle} - \phi_{\left\langle -\Delta\overline{\omega}\frac{\partial\{q'\}}{\partial p}\right\rangle}\right) \\ \cos\left(\phi_{\left\langle -\omega\frac{\partial q}{\partial p}\right\rangle} - \phi_{\left\langle -\overline{\omega}\frac{\partial\{\Delta q'\}}{\partial p}\right\rangle}\right) \\ \cos\left(\phi_{\left\langle -\omega\frac{\partial q}{\partial p}\right\rangle} - \phi_{\left\langle -\{\Delta\omega'\}\frac{\partial\overline{q}}{\partial p}\right\rangle}\right) \\ \cos\left(\phi_{\left\langle -\omega\frac{\partial q}{\partial p}\right\rangle} - \phi_{\left\langle -\{\omega'\}\frac{\partial\Delta\overline{q}}{\partial p}\right\rangle}\right) \\ A_{\left\langle -\Delta\overline{\omega}\frac{\partial\{q'\}}{\partial p}\right\rangle}\sin\left(\phi_{\left\langle -\omega\frac{\partial q}{\partial p}\right\rangle} - \phi_{\left\langle -\Delta\overline{\omega}\frac{\partial\{q'\}}{\partial p}\right\rangle}\right) \\ A_{\left\langle -\overline{\omega}\frac{\partial\{\Delta q'\}}{\partial p}\right\rangle}\sin\left(\phi_{\left\langle -\omega\frac{\partial q}{\partial p}\right\rangle} - \phi_{\left\langle -\overline{\omega}\frac{\partial\{\Delta q'\}}{\partial p}\right\rangle}\right) \\ A_{\left\langle -\{\Delta\omega'\}\frac{\partial\overline{q}}{\partial p}\right\rangle}\sin\left(\phi_{\left\langle -\omega\frac{\partial q}{\partial p}\right\rangle} - \phi_{\left\langle -\{\Delta\omega'\}\frac{\partial\overline{q}}{\partial p}\right\rangle}\right) \\ A_{\left\langle -\{\omega'\}\frac{\partial\Delta\overline{q}}{\partial p}\right\rangle}\sin\left(\phi_{\left\langle -\omega\frac{\partial q}{\partial p}\right\rangle} - \phi_{\left\langle -\{\omega'\}\frac{\partial\Delta\overline{q}}{\partial p}\right\rangle}\right) \end{bmatrix}^{\top} \begin{bmatrix} \Delta A_{\left\langle -\Delta\overline{\omega}\frac{\partial\{q'\}}{\partial p}\right\rangle} \\ \Delta A_{\left\langle -\overline{\omega}\frac{\partial\{\Delta q'\}}{\partial p}\right\rangle} \\ \Delta A_{\left\langle -\{\Delta\omega'\}\frac{\partial\overline{q}}{\partial p}\right\rangle} \\ \Delta A_{\left\langle -\{\omega'\}\frac{\partial\Delta\overline{q}}{\partial p}\right\rangle} \\ \Delta\phi_{\left\langle -\Delta\overline{\omega}\frac{\partial\{q'\}}{\partial p}\right\rangle} \\ \Delta\phi_{\left\langle -\overline{\omega}\frac{\partial\{\Delta q'\}}{\partial p}\right\rangle} \\ \Delta\phi_{\left\langle -\{\Delta\omega'\}\frac{\partial\overline{q}}{\partial p}\right\rangle} \\ \Delta\phi_{\left\langle -\{\omega'\}\frac{\partial\Delta\overline{q}}{\partial p}\right\rangle} \end{bmatrix} \tag{B5}$$

$$\Delta\phi_{\left\langle -\omega\frac{\partial q}{\partial p}\right\rangle} = \frac{1}{A_{\left\langle -\omega\frac{\partial q}{\partial p}\right\rangle}} \begin{bmatrix} \sin\left(\phi_{\left\langle -\Delta\overline{\omega}\frac{\partial\{q'\}}{\partial p}\right\rangle} - \phi_{\left\langle -\omega\frac{\partial q}{\partial p}\right\rangle}\right) \\ \sin\left(\phi_{\left\langle -\overline{\omega}\frac{\partial\{\Delta q'\}}{\partial p}\right\rangle} - \phi_{\left\langle -\omega\frac{\partial q}{\partial p}\right\rangle}\right) \\ \sin\left(\phi_{\left\langle -\{\Delta\omega'\}\frac{\partial\overline{q}}{\partial p}\right\rangle} - \phi_{\left\langle -\omega\frac{\partial q}{\partial p}\right\rangle}\right) \\ \sin\left(\phi_{\left\langle -\{\omega'\}\frac{\partial\Delta\overline{q}}{\partial p}\right\rangle} - \phi_{\left\langle -\omega\frac{\partial q}{\partial p}\right\rangle}\right) \\ A_{\left\langle -\Delta\overline{\omega}\frac{\partial\{q'\}}{\partial p}\right\rangle}\cos\left(\phi_{\left\langle -\Delta\overline{\omega}\frac{\partial\{q'\}}{\partial p}\right\rangle} - \phi_{\left\langle -\omega\frac{\partial q}{\partial p}\right\rangle}\right) \\ A_{\left\langle -\overline{\omega}\frac{\partial\{\Delta q'\}}{\partial p}\right\rangle}\cos\left(\phi_{\left\langle -\overline{\omega}\frac{\partial\{\Delta q'\}}{\partial p}\right\rangle} - \phi_{\left\langle -\omega\frac{\partial q}{\partial p}\right\rangle}\right) \\ A_{\left\langle -\{\Delta\omega'\}\frac{\partial\overline{q}}{\partial p}\right\rangle}\cos\left(\phi_{\left\langle -\{\Delta\omega'\}\frac{\partial\overline{q}}{\partial p}\right\rangle} - \phi_{\left\langle -\omega\frac{\partial q}{\partial p}\right\rangle}\right) \\ A_{\left\langle -\{\omega'\}\frac{\partial\Delta\overline{q}}{\partial p}\right\rangle}\cos\left(\phi_{\left\langle -\{\omega'\}\frac{\partial\Delta\overline{q}}{\partial p}\right\rangle} - \phi_{\left\langle -\omega\frac{\partial q}{\partial p}\right\rangle}\right) \end{bmatrix}^{\top} \begin{bmatrix} \Delta A_{\left\langle -\Delta\overline{\omega}\frac{\partial\{q'\}}{\partial p}\right\rangle} \\ \Delta A_{\left\langle -\overline{\omega}\frac{\partial\{\Delta q'\}}{\partial p}\right\rangle} \\ \Delta A_{\left\langle -\{\Delta\omega'\}\frac{\partial\overline{q}}{\partial p}\right\rangle} \\ \Delta A_{\left\langle -\{\omega'\}\frac{\partial\Delta\overline{q}}{\partial p}\right\rangle} \\ \Delta\phi_{\left\langle -\Delta\overline{\omega}\frac{\partial\{q'\}}{\partial p}\right\rangle} \\ \Delta\phi_{\left\langle -\overline{\omega}\frac{\partial\{\Delta q'\}}{\partial p}\right\rangle} \\ \Delta\phi_{\left\langle -\{\Delta\omega'\}\frac{\partial\overline{q}}{\partial p}\right\rangle} \\ \Delta\phi_{\left\langle -\{\omega'\}\frac{\partial\Delta\overline{q}}{\partial p}\right\rangle} \end{bmatrix} \tag{B6}$$

Since we are interested in what effect the various changes of annual mean, amplitude, and phase of ω and $\partial q/\partial p$ have on $\left\langle -\omega\frac{\partial q}{\partial p}\right\rangle$, we further decompose the terms $A_{\left\langle -\overline{\omega}\frac{\partial\{\Delta q'\}}{\partial p}\right\rangle}$, $A_{\left\langle -\{\Delta\omega'\}\frac{\partial\overline{q}}{\partial p}\right\rangle}$, $\phi_{\left\langle -\overline{\omega}\frac{\partial\{\Delta q'\}}{\partial p}\right\rangle}$, and $\phi_{\left\langle -\{\Delta\omega'\}\frac{\partial\overline{q}}{\partial p}\right\rangle}$ each into separate terms relating to the change in amplitude or phase of $\partial q/\partial p$ or ω as follows:

$$\Delta A_{\left\langle -\overline{\omega}\frac{\partial\{\Delta q'\}}{\partial p}\right\rangle} = \Delta A_{\left\langle -\overline{\omega}\frac{\partial\{\Delta q'\}}{\partial p}\right\rangle;\Delta A_{\partial q/\partial p}} + \Delta A_{\left\langle -\overline{\omega}\frac{\partial\{\Delta q'\}}{\partial p}\right\rangle;\Delta\phi_{\partial q/\partial p}} \tag{B7}$$

$$\Delta A_{\left\langle -\{\Delta\omega'\}\frac{\partial\overline{q}}{\partial p}\right\rangle} = \Delta A_{\left\langle -\{\Delta\omega'\}\frac{\partial\overline{q}}{\partial p}\right\rangle;\Delta A_{\omega}} + \Delta A_{\left\langle -\{\Delta\omega'\}\frac{\partial\overline{q}}{\partial p}\right\rangle;\Delta\phi_{\omega}} \tag{B8}$$

$$\Delta\phi_{\left\langle -\overline{\omega}\frac{\partial\{\Delta q'\}}{\partial p}\right\rangle} = \Delta\phi_{\left\langle -\overline{\omega}\frac{\partial\{\Delta q'\}}{\partial p}\right\rangle;\Delta A_{\partial q/\partial p}} + \Delta\phi_{\left\langle -\overline{\omega}\frac{\partial\{\Delta q'\}}{\partial p}\right\rangle;\Delta\phi_{\partial q/\partial p}} \tag{B9}$$

$$\Delta\phi_{\left\langle -\{\Delta\omega'\}\frac{\partial\overline{q}}{\partial p}\right\rangle} = \Delta\phi_{\left\langle -\{\Delta\omega'\}\frac{\partial\overline{q}}{\partial p}\right\rangle;\Delta A_{\omega}} + \Delta\phi_{\left\langle -\{\Delta\omega'\}\frac{\partial\overline{q}}{\partial p}\right\rangle;\Delta\phi_{\omega}}, \tag{B10}$$

where, for example, $\Delta A_{\left\langle -\overline{\omega}\frac{\partial\{\Delta q'\}}{\partial p}\right\rangle;\Delta A_{\partial q/\partial p}}$ is the effect of a change in the amplitude of $\partial q/\partial p$ on $\Delta A_{\left\langle -\overline{\omega}\frac{\partial\{\Delta q'\}}{\partial p}\right\rangle}$. With this in mind we can write the effect that changes in various components changes of ω and q have on $A_{\left\langle -\omega\frac{\partial q}{\partial p}\right\rangle}$ and $\phi_{\left\langle -\omega\frac{\partial q}{\partial p}\right\rangle}$ as follows.

$$
\begin{bmatrix}
\Delta A_{\left\langle -\omega \frac{\partial q}{\partial p} \right\rangle ; \overline{\omega}} \\
\Delta A_{\left\langle -\omega \frac{\partial q}{\partial p} \right\rangle ; A_\omega} \\
\Delta A_{\left\langle -\omega \frac{\partial q}{\partial p} \right\rangle ; \phi_\omega} \\
\Delta A_{\left\langle -\omega \frac{\partial q}{\partial p} \right\rangle ; \partial \overline{q}/\partial p} \\
\Delta A_{\left\langle -\omega \frac{\partial q}{\partial p} \right\rangle ; A_{\partial q/\partial p}} \\
\Delta A_{\left\langle -\omega \frac{\partial q}{\partial p} \right\rangle ; \phi_{\partial q/\partial p}}
\end{bmatrix}
=
\tag{B11}
$$

$$
\begin{bmatrix}
\cos\left(\phi_{\left\langle -\omega \frac{\partial q}{\partial p} \right\rangle} - \phi_{\left\langle -\Delta\overline{\omega} \frac{\partial \{q'\}}{\partial p} \right\rangle}\right) \Delta A_{\left\langle -\Delta\overline{\omega} \frac{\partial \{q'\}}{\partial p} \right\rangle} + A_{\left\langle -\Delta\overline{\omega} \frac{\partial \{q'\}}{\partial p} \right\rangle} \sin\left(\phi_{\left\langle -\omega \frac{\partial q}{\partial p} \right\rangle} - \phi_{\left\langle -\Delta\overline{\omega} \frac{\partial \{q'\}}{\partial p} \right\rangle}\right) \Delta \phi_{\left\langle -\Delta\overline{\omega} \frac{\partial \{q'\}}{\partial p} \right\rangle} \\
\cos\left(\phi_{\left\langle -\omega \frac{\partial q}{\partial p} \right\rangle} - \phi_{\left\langle -\{\Delta\omega'\} \frac{\partial \overline{q}}{\partial p} \right\rangle}\right) \Delta A_{\left\langle -\{\Delta\omega'\} \frac{\partial \overline{q}}{\partial p} \right\rangle ; \Delta A_\omega} + A_{\left\langle -\{\Delta\omega'\} \frac{\partial \overline{q}}{\partial p} \right\rangle} \sin\left(\phi_{\left\langle -\omega \frac{\partial q}{\partial p} \right\rangle} - \phi_{\left\langle -\{\Delta\omega'\} \frac{\partial \overline{q}}{\partial p} \right\rangle}\right) \Delta \phi_{\left\langle -\{\Delta\omega'\} \frac{\partial \overline{q}}{\partial p} \right\rangle ; \Delta A_\omega} \\
\cos\left(\phi_{\left\langle -\omega \frac{\partial q}{\partial p} \right\rangle} - \phi_{\left\langle -\{\Delta\omega'\} \frac{\partial \overline{q}}{\partial p} \right\rangle}\right) \Delta A_{\left\langle -\{\Delta\omega'\} \frac{\partial \overline{q}}{\partial p} \right\rangle ; \Delta \phi_\omega} + A_{\left\langle -\{\Delta\omega'\} \frac{\partial \overline{q}}{\partial p} \right\rangle} \sin\left(\phi_{\left\langle -\omega \frac{\partial q}{\partial p} \right\rangle} - \phi_{\left\langle -\{\Delta\omega'\} \frac{\partial \overline{q}}{\partial p} \right\rangle}\right) \Delta \phi_{\left\langle -\{\Delta\omega'\} \frac{\partial \overline{q}}{\partial p} \right\rangle ; \Delta \phi_\omega} \\
\cos\left(\phi_{\left\langle -\omega \frac{\partial q}{\partial p} \right\rangle} - \phi_{\left\langle -\{\omega'\} \frac{\partial \Delta\overline{q}}{\partial p} \right\rangle}\right) \Delta A_{\left\langle -\{\omega'\} \frac{\partial \Delta\overline{q}}{\partial p} \right\rangle} + A_{\left\langle -\{\omega'\} \frac{\partial \Delta\overline{q}}{\partial p} \right\rangle} \sin\left(\phi_{\left\langle -\omega \frac{\partial q}{\partial p} \right\rangle} - \phi_{\left\langle -\{\omega'\} \frac{\partial \Delta\overline{q}}{\partial p} \right\rangle}\right) \Delta \phi_{\left\langle -\{\omega'\} \frac{\partial \Delta\overline{q}}{\partial p} \right\rangle} \\
\cos\left(\phi_{\left\langle -\omega \frac{\partial q}{\partial p} \right\rangle} - \phi_{\left\langle -\overline{\omega} \frac{\partial \{\Delta q'\}}{\partial p} \right\rangle}\right) \Delta A_{\left\langle -\overline{\omega} \frac{\partial \{\Delta q'\}}{\partial p} \right\rangle ; \Delta A_q} + A_{\left\langle -\overline{\omega} \frac{\partial \{\Delta q'\}}{\partial p} \right\rangle} \sin\left(\phi_{\left\langle -\omega \frac{\partial q}{\partial p} \right\rangle} - \phi_{\left\langle -\overline{\omega} \frac{\partial \{\Delta q'\}}{\partial p} \right\rangle}\right) \Delta \phi_{\left\langle -\overline{\omega} \frac{\partial \{\Delta q'\}}{\partial p} \right\rangle ; \Delta A_q} \\
\cos\left(\phi_{\left\langle -\omega \frac{\partial q}{\partial p} \right\rangle} - \phi_{\left\langle -\overline{\omega} \frac{\partial \{\Delta q'\}}{\partial p} \right\rangle}\right) \Delta A_{\left\langle -\overline{\omega} \frac{\partial \{\Delta q'\}}{\partial p} \right\rangle ; \Delta \phi_q} + A_{\left\langle -\overline{\omega} \frac{\partial \{\Delta q'\}}{\partial p} \right\rangle} \sin\left(\phi_{\left\langle -\omega \frac{\partial q}{\partial p} \right\rangle} - \phi_{\left\langle -\overline{\omega} \frac{\partial \{\Delta q'\}}{\partial p} \right\rangle}\right) \Delta \phi_{\left\langle -\overline{\omega} \frac{\partial \{\Delta q'\}}{\partial p} \right\rangle ; \Delta \phi_q}
\end{bmatrix}
$$

$$
\begin{bmatrix}
\Delta \phi_{\left\langle -\omega \frac{\partial q}{\partial p} \right\rangle ; \overline{\omega}} \\
\Delta \phi_{\left\langle -\omega \frac{\partial q}{\partial p} \right\rangle ; A_\omega} \\
\Delta \phi_{\left\langle -\omega \frac{\partial q}{\partial p} \right\rangle ; \phi_\omega} \\
\Delta \phi_{\left\langle -\omega \frac{\partial q}{\partial p} \right\rangle ; \partial \overline{q}/\partial p} \\
\Delta \phi_{\left\langle -\omega \frac{\partial q}{\partial p} \right\rangle ; A_{\partial q/\partial p}} \\
\Delta \phi_{\left\langle -\omega \frac{\partial q}{\partial p} \right\rangle ; \phi_{\partial q/\partial p}}
\end{bmatrix}
= \frac{1}{A_{\left\langle -\omega \frac{\partial q}{\partial p} \right\rangle}} \times
\tag{B12}
$$

$$
\begin{bmatrix}
\sin\left(\phi_{\left\langle -\Delta\overline{\omega} \frac{\partial \{q'\}}{\partial p} \right\rangle} - \phi_{\left\langle -\omega \frac{\partial q}{\partial p} \right\rangle}\right) \Delta A_{\left\langle -\Delta\overline{\omega} \frac{\partial \{q'\}}{\partial p} \right\rangle} + A_{\left\langle -\Delta\overline{\omega} \frac{\partial \{q'\}}{\partial p} \right\rangle} \cos\left(\phi_{\left\langle -\Delta\overline{\omega} \frac{\partial \{q'\}}{\partial p} \right\rangle} - \phi_{\left\langle -\omega \frac{\partial q}{\partial p} \right\rangle}\right) \Delta \phi_{\left\langle -\Delta\overline{\omega} \frac{\partial \{q'\}}{\partial p} \right\rangle} \\
\sin\left(\phi_{\left\langle -\{\Delta\omega'\} \frac{\partial \overline{q}}{\partial p} \right\rangle} - \phi_{\left\langle -\omega \frac{\partial q}{\partial p} \right\rangle}\right) \Delta A_{\left\langle -\{\Delta\omega'\} \frac{\partial \overline{q}}{\partial p} \right\rangle ; \Delta A_\omega} + A_{\left\langle -\{\Delta\omega'\} \frac{\partial \overline{q}}{\partial p} \right\rangle} \cos\left(\phi_{\left\langle -\{\Delta\omega'\} \frac{\partial \overline{q}}{\partial p} \right\rangle} - \phi_{\left\langle -\omega \frac{\partial q}{\partial p} \right\rangle}\right) \Delta \phi_{\left\langle -\{\Delta\omega'\} \frac{\partial \overline{q}}{\partial p} \right\rangle ; \Delta A_\omega} \\
\sin\left(\phi_{\left\langle -\{\Delta\omega'\} \frac{\partial \overline{q}}{\partial p} \right\rangle} - \phi_{\left\langle -\omega \frac{\partial q}{\partial p} \right\rangle}\right) \Delta A_{\left\langle -\{\Delta\omega'\} \frac{\partial \overline{q}}{\partial p} \right\rangle ; \Delta \phi_\omega} + A_{\left\langle -\{\Delta\omega'\} \frac{\partial \overline{q}}{\partial p} \right\rangle} \cos\left(\phi_{\left\langle -\{\Delta\omega'\} \frac{\partial \overline{q}}{\partial p} \right\rangle} - \phi_{\left\langle -\omega \frac{\partial q}{\partial p} \right\rangle}\right) \Delta \phi_{\left\langle -\{\Delta\omega'\} \frac{\partial \overline{q}}{\partial p} \right\rangle ; \Delta \phi_\omega} \\
\sin\left(\phi_{\left\langle -\{\omega'\} \frac{\partial \Delta\overline{q}}{\partial p} \right\rangle} - \phi_{\left\langle -\omega \frac{\partial q}{\partial p} \right\rangle}\right) \Delta A_{\left\langle -\{\omega'\} \frac{\partial \Delta\overline{q}}{\partial p} \right\rangle} + A_{\left\langle -\{\omega'\} \frac{\partial \Delta\overline{q}}{\partial p} \right\rangle} \cos\left(\phi_{\left\langle -\{\omega'\} \frac{\partial \Delta\overline{q}}{\partial p} \right\rangle} - \phi_{\left\langle -\omega \frac{\partial q}{\partial p} \right\rangle}\right) \Delta \phi_{\left\langle -\{\omega'\} \frac{\partial \Delta\overline{q}}{\partial p} \right\rangle} \\
\sin\left(\phi_{\left\langle -\overline{\omega} \frac{\partial \{\Delta q'\}}{\partial p} \right\rangle} - \phi_{\left\langle -\omega \frac{\partial q}{\partial p} \right\rangle}\right) \Delta A_{\left\langle -\overline{\omega} \frac{\partial \{\Delta q'\}}{\partial p} \right\rangle ; \Delta A_q} + A_{\left\langle -\overline{\omega} \frac{\partial \{\Delta q'\}}{\partial p} \right\rangle} \cos\left(\phi_{\left\langle -\overline{\omega} \frac{\partial \{\Delta q'\}}{\partial p} \right\rangle} - \phi_{\left\langle -\omega \frac{\partial q}{\partial p} \right\rangle}\right) \Delta \phi_{\left\langle -\overline{\omega} \frac{\partial \{\Delta q'\}}{\partial p} \right\rangle ; \Delta A_q} \\
\sin\left(\phi_{\left\langle -\overline{\omega} \frac{\partial \{\Delta q'\}}{\partial p} \right\rangle} - \phi_{\left\langle -\omega \frac{\partial q}{\partial p} \right\rangle}\right) \Delta A_{\left\langle -\overline{\omega} \frac{\partial \{\Delta q'\}}{\partial p} \right\rangle ; \Delta \phi_q} + A_{\left\langle -\overline{\omega} \frac{\partial \{\Delta q'\}}{\partial p} \right\rangle} \cos\left(\phi_{\left\langle -\overline{\omega} \frac{\partial \{\Delta q'\}}{\partial p} \right\rangle} - \phi_{\left\langle -\omega \frac{\partial q}{\partial p} \right\rangle}\right) \Delta \phi_{\left\langle -\overline{\omega} \frac{\partial \{\Delta q'\}}{\partial p} \right\rangle ; \Delta \phi_q}
\end{bmatrix}
$$

REFERENCES

Biasutti, M., 2013: Forced Sahel rainfall trends in the CMIP5 archive. *Journal of Geophysical Research: Atmospheres*, doi:10.1002/jgrd.50206.

Biasutti, M., D. S. Battisti, and E. S. Sarachik, 2003: The annual cycle over the tropical Atlantic, South America, and Africa. *Journal of Climate*, **16 (15)**, 2491–2508, doi:10.1175/1520-0442(2003)016⟨2491:TACOTT⟩2.0.CO;2.

Biasutti, M., D. S. Battisti, and E. S. Sarachik, 2004: Mechanisms controlling the annual cycle of precipitation in the tropical Atlantic sector in an atmospheric GCM. *Journal of Climate*, **17 (24)**, 4708–4723, doi:10.1175/JCLI-3235.1.

Biasutti, M. and A. Sobel, 2009: Delayed Sahel rainfall and global seasonal cycle in a warmer climate. *Geophys. Res. Lett.*, **36**, doi:10.1029/2009GL041303.

Cess, R. D., et al., 1990: Intercomparison and interpretation of climate feedback processes in 19 atmospheric general circulation models. *Journal of Geophysical Research: Atmospheres*, **95 (D10)**, 16 601–16 615, doi:10.1029/JD095iD10p16601.

Chiang, J. C. H. and A. H. Sobel, 2002: Tropical tropospheric temperature variations caused by ENSO and their influence on the remote tropical climate. *Journal of Climate*, **15 (18)**, 2616–2631, doi:10.1175/1520-0442(2002)015⟨2616:TTTVCB⟩2.0.CO;2.

Chou, C. and C.-W. Lan, 2011: Changes in the annual range of precipitation under global warming. *Journal of Climate*, **25 (1)**, 222–235, doi:10.1175/JCLI-D-11-00097.1.

Chou, C. and J. D. Neelin, 2004: Mechanisms of global warming impacts on regional tropical precipitation. *Journal of Climate*, **17 (13)**, 2688–2701, doi:10.1175/1520-0442(2004)017⟨2688:MOGWIO⟩2.0.CO;2.

Chou, C., J.-Y. Tu, and P.-H. Tan, 2007: Asymmetry of tropical precipitation change under global warming. *Geophys. Res. Lett.*, **34 (17)**, L17 708, doi:10.1029/2007GL030327.

Dwyer, J. G., M. Biasutti, and A. H. Sobel, 2012: Projected changes in the seasonal cycle of surface temperature. *Journal of Climate*, **25 (18)**, 6359–6374, doi:10.1175/JCLI-D-11-00741.1.

Emanuel, K. and A. H. Sobel, 2013: Response of tropical sea surface temperature, precipitation, and tropical cyclone-related variables to changes in global and local forcing. *Journal of Advances in Modeling Earth Systems*, submitted.

Fu, R., R. E. Dickinson, M. Chen, and H. Wang, 2001: How do tropical sea surface temperatures influence the seasonal distribution of precipitation in the equatorial Amazon? *Journal of Climate*, **14 (20)**, 4003–4026, doi:10.1175/1520-0442(2001)014⟨4003:HDTSST⟩2.0.CO;2.

Fu, X. and B. Wang, 2004: Differences of boreal summer intraseasonal oscillations simulated in an atmosphere–ocean coupled model and an atmosphere-only model. *Journal of Climate*, **17 (6)**, 1263–1271, doi:10.1175/1520-0442(2004)017⟨1263:DOBSIO⟩2.0.CO;2.

Gent, P. R., et al., 2011: The Community Climate System Model Version 4. *Journal of Climate*, **24 (19)**, 4973–4991, doi:10.1175/2011JCLI4083.1.

Held, I. and B. Soden, 2006: Robust responses of the hydrological cycle to global warming. *Journal of Climate*, **19 (21)**, 5686–5699.

Huang, P., S.-P. Xie, K. Hu, G. Huang, and R. Huang, 2013: Patterns of tropical rainfall response to global warming: How to get wetter? *Nature Geoscience*, in press.

Hurrell, J. W., J. J. Hack, D. Shea, J. M. Caron, and J. Rosinski, 2008: A new sea surface temperature and sea ice boundary dataset for the community atmosphere model. *Journal of Climate*, **21 (19)**, 5145–5153, doi:10.1175/2008JCLI2292.1.

Kitoh, A. and O. Arakawa, 1999: On overestimation of tropical precipitation by an atmospheric GCM with prescribed SST. *Geophys. Res. Lett.*, **26 (19)**, 2965–2968, doi:10.1029/1999GL900616.

Kutzbach, J., 1967: Empirical eigenvectors of sea-level pressure, surface temperature and precipitation complexes over North America. *J. Appl. Meteor.*, **6**, 791–802.

Li, T. and S. G. H. Philander, 1997: On the seasonal cycle of the equatorial Atlantic Ocean. *Journal of Climate*, **10 (4)**, 813–817, doi:10.1175/1520-0442(1997)010⟨0813:OTSCOT⟩2.0.CO;2.

Lin, J.-L., 2007: The double-ITCZ problem in IPCC AR4 coupled GCMs: Ocean–atmosphere feedback analysis. *Journal of Climate*, **20 (18)**, 4497–4525, doi:10.1175/JCLI4272.1.

Liu, C., R. P. Allan, and G. J. Huffman, 2012: Co-variation of temperature and precipitation in CMIP5 models and satellite observations. *Geophys. Res. Lett.*, **39 (13)**, L13 803, doi:10.1029/2012GL052093.

Meehl, G., C. Covey, T. Delworth, M. Latif, B. McAvaney, J. Mitchell, R. Stouffer, and K. Taylor, 2007: The WCRP CMIP3 multimodel dataset. *Bull. Am. Meteorol. Soc.*, **88**, 1383–1394.

Seager, R. and N. Henderson, 2013: Diagnostic computation of moisture budgets in the ERA-Interim reanalysis with reference to analysis of CMIP-archived atmospheric model data. *Journal of Climate*, submitted.

Seth, A., S. Rauscher, M. Biasutti, A. Giannini, S. Camargo, and M. Rojas, 2013: CMIP5 projected changes in the annual cycle of precipitation in monsoon regions. *Journal of Climate*, accepted.

Seth, A., S. Rauscher, M. Rojas, A. Giannini, and S. Camargo, 2011: Enhanced spring convective barrier for monsoons in a warmer world? *Clim. Change*, **104 (2)**, 403–414, doi:10.1007/s10584-010-9973-8.

Shukla, J. and M. Fennessy, 1994: Simulation and predictability of monsoons. Proceedings of the international conference on monsoon variability and prediction. Tech. rep., WCRP-84, World Climate Research Program, Geneva, Switzerland. 567-575.

Sobel, A. and S. Camargo, 2011: Projected future seasonal changes in tropical summer climate. *J. Climate*, **24**, 473–487, doi:10.1175/2010JCLI3748.1.

Tan, P.-H., C. Chou, and J.-Y. Tu, 2008: Mechanisms of global warming impacts on robustness of tropical precipitation asymmetry. *Journal of Climate*, **21 (21)**, 5585–5602, doi:10.1175/2008JCLI2154.1.

Taylor, K. E., R. J. Stouffer, and G. A. Meehl, 2011: An overview of CMIP5 and the experiment design. *Bulletin of the American Meteorological Society*, **93 (4)**, 485–498, doi:10.1175/BAMS-D-11-00094.1.

Trenberth, K. E., D. P. Stepaniak, and J. M. Caron, 2000: The global monsoon as seen through the divergent atmospheric circulation. *Journal of Climate*, **13 (22)**, 3969–3993, doi:10.1175/1520-0442(2000)013⟨3969:TGMAST⟩2.0.CO;2.

Vecchi, G. A., B. J. Soden, A. T. Wittenberg, I. M. Held, A. Leetmaa, and M. J. Harrison, 2006: Weakening of tropical pacific atmospheric circulation due to anthropogenic forcing. *Nature*, **441 (7089)**, 73–76.

Wu, R. and B. Kirtman, 2005: Roles of Indian and Pacific Ocean air–sea coupling in tropical atmospheric variability. *Climate Dynamics*, **25 (2-3)**, 155–170.

Wu, R. and B. Kirtman, 2007: Regimes of seasonal air–sea interaction and implications for performance of forced simulations. *Climate Dynamics*, **29 (4)**, 393–410.

Xie, S.-P., C. Deser, G. A. Vecchi, J. Ma, H. Teng, and A. T. Wittenberg, 2010: Global warming pattern formation: Sea surface temperature and rainfall. *Journal of Climate*, **23 (4)**, 966–986, doi:10.1175/2009JCLI3329.1.

List of Tables

Model	Group, Country
ACCESS1-3	CSIRO-BOM, Australia
BCC-CSM1-1	BCC, China
BCC-CSM1-1-m	BCC, China
BNU-ESM	GCESS, China
CanESM2	CCCma, Canada
CCSM4	NCAR, USA
CESM1-BGC	NSF-DOE-NCAR, USA
CESM1-CAM5	NSF-DOE-NCAR, USA
CESM1-WACCM	NSF-DOE-NCAR, USA
CMCC-CM	CMCC, Italy
CMCC-CMS	CMCC, Italy
CNRM-CM5	CNRM-CERFACS, France
CSIRO-Mk3-6-0	CSIRO-QCCCE, Australia
FGOALS-g2	LASG-CESS, China
FGOALS-s2	LASG-IAP, China
FIO-ESM	FIO, China
GFDL-CM3	NOAA-GFDL, USA
GFDL-ESM2G	NOAA-GFDL, USA
GFDL-ESM2M	NOAA-GFDL, USA
GISS-E2-R	NASA GISS, USA
GISS-E2-H	NASA GISS, USA
HadGEM2-CC	MOHC, UK
HadGEM2-ES	MOHC, UK
INM-CM4	INM, Russia
IPSL-CM5A-LR	IPSL, France
IPSL-CM5A-MR	IPSL, France
IPSL-CM5B-LR	IPSL, France
MIROC-ESM	MIROC, Japan
MIROC-ESM-CHEM	MIROC, Japan
MIROC5	MIROC, Japan
MPI-ESM-LR	MPI-M, Germany
MPI-ESM-MR	MPI-M, Germany
MRI-CGCM3	MRI, Japan
NorESM1-M	NCC, Norway
NorESM1-ME	NCC, Norway

Table 1. The 35 CMIP5 models used in this study.

	SST		Ocean Precip.		Land Precip.	
Δ Annual Mean	2.9 K	(35)	0.2 mm day^{-1}	(35)	0.1 mm day^{-1}	(27)
Δ Amplitude	4.2%	(33)	15.5%	(34)	8.2%	(35)
Δ Phase	1.1 days	(29)	2.7 days	(27)	3.5 days	(34)

TABLE 2. Multi-model mean changes in the annual mean, phase, and amplitude over ocean and land in the tropics (25°S–25°N) for the CMIP5 models between 2080–2099 relative to 1980–1999. Seasonal changes were calculated using EOF analysis. Numbers in parentheses indicate the number of models projecting changes of the same sign as the mean for each quantity out of a total of 35 models.

	Ocean		Land	
	Calculated A_P	Calculated ϕ_P	Calculated A_P	Calculated ϕ_P
$\Delta\overline{SST}_{CMIP5} = 2.9$ K	22.7%	4.7 days	7.6%	1.7 days
$\Delta A_{SST,CMIP5}$=4.2%	2.4%	1.4 days	0.8%	0.8 days
$\Delta\phi_{SST,CMIP5} = 1.1$ days	-0.2%	1.1 days	-0.3%	0.4 days
Total Calculated	24.9%	7.2 days	8.1%	2.9 days
Acutal CMIP5	15.5%	2.7 days	8.2%	3.5 days

Table 3. Calculated changes in amplitude and phase in precipitation for both ocean and land given changes in the annual mean and annual cycle of SST in the CMIP5 models. We used the UW simulation to calculate the changes due to an annual mean SST increase and the sensitivity of the modified seasonality experiments to calculate the changes due to a phase or amplitude change. Total calculated changes are the sum of the individual contributions.

List of Figures

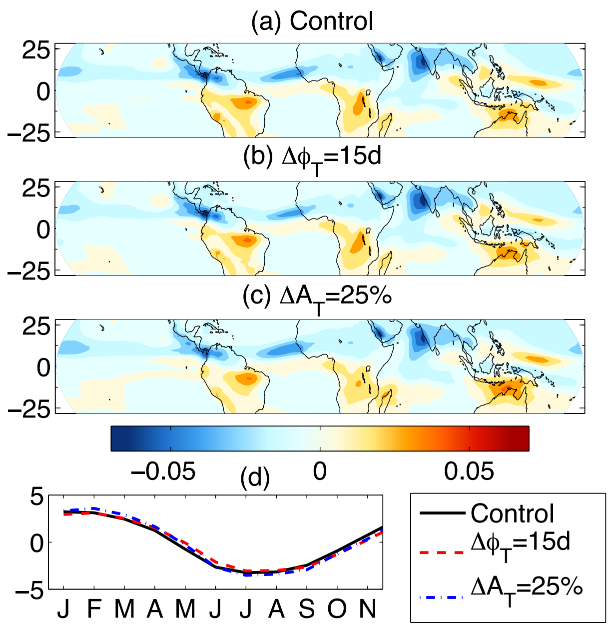

Fig. 1. The first EOF of tropical precipitation, representing the annual cycle, for the control simulation (a), a simulation forced with a 15 day phase delay of SST (b), and a simulation forced with a 25% amplitude increase of SST (c). We also plot the PC1s associated with each EOF in (d).

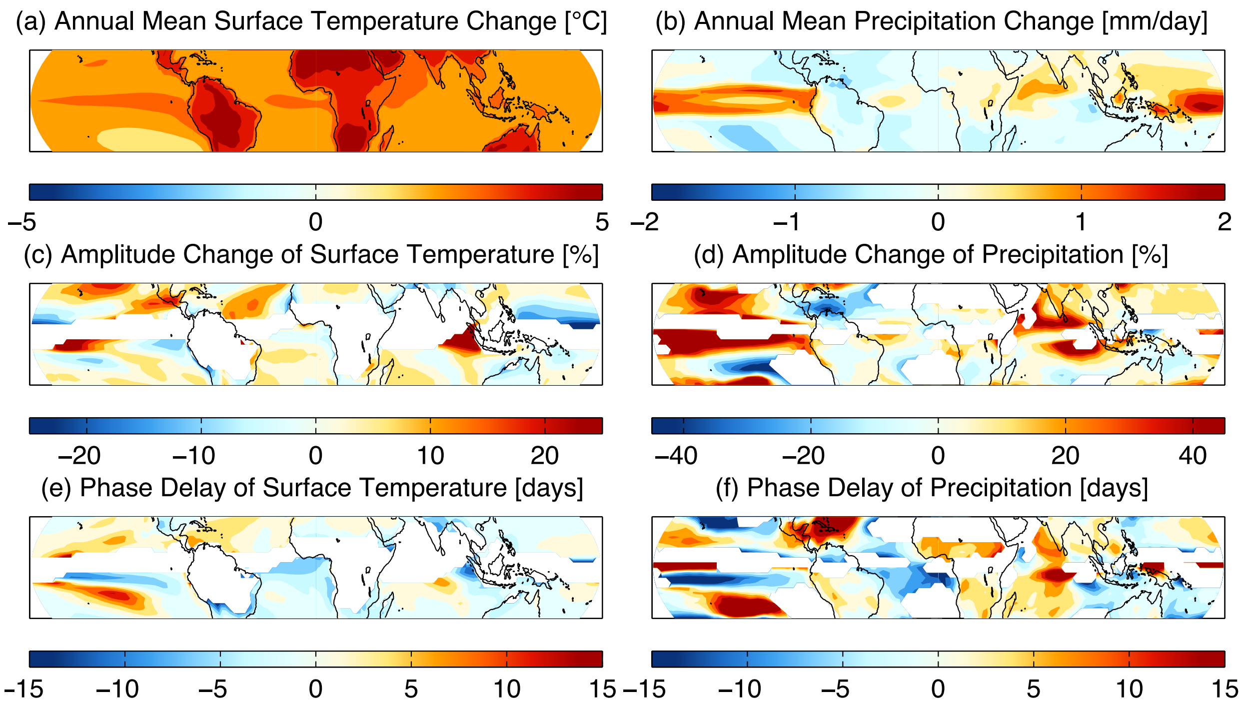

Fig. 2. The CMIP5 RCP8.5 multi-model mean change between 2080-2099 and 1980-1999 for annual mean temperature (a) and precipitation (b), amplitude change of the annual cycle of temperature (c) and precipitation (d), and phase delay of the annual cycle of temperature (e) and precipitation (f). Any location where the first harmonic makes up less than 80% or 50% of the total variance for temperature and precipitation, respectively, is not shaded. Additionally, for (d) and (f) we only shade grid points that have at least an annual mean precipitation of 1 mm day^{-1}.

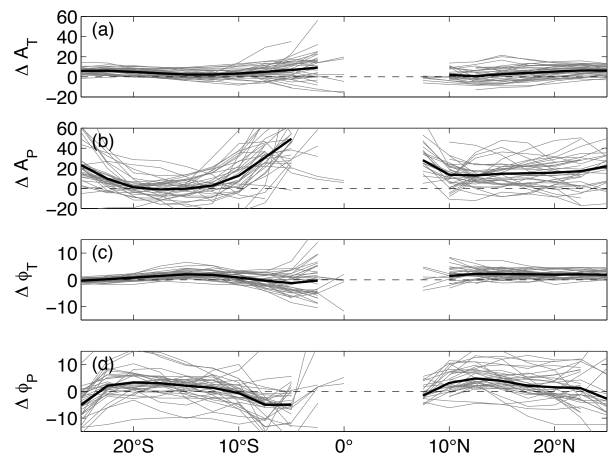

FIG. 3. Zonal mean, oceanic changes for the CMIP5 models between 2080–2099 and 1980–1999 for (a) the amplitude of SST, (b) the amplitude of precipitation, (c) the phase of SST, and (d) the phase of precipitation. The thick black line indicates the multi-model mean, and the thin gray lines the individual models. Values were calculated by first zonally averaging over ocean and then calculating seasonal characteristics and are only plotted for where the annual harmonic is responsible for at least 80% of the total variance. Units for amplitude are percent and units for phase are days.

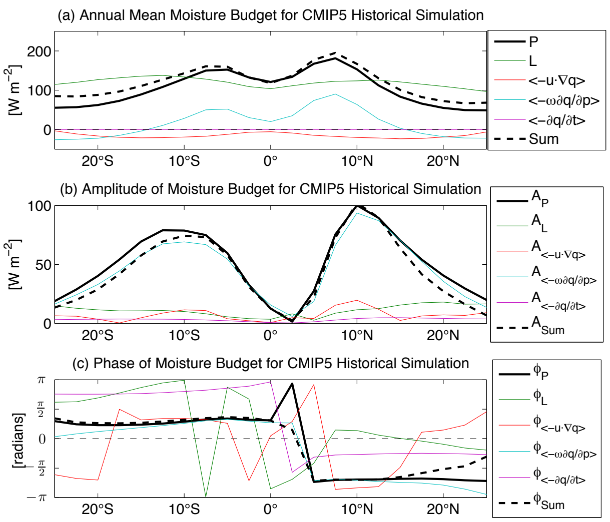

FIG. 4. Annual mean (a), amplitude (b), and phase (c) of the terms in the moisture budget (Equation 3) for the multi-model mean of the CMIP5 simulations. The solid, thick, black line is precipitation and the dashed, thick, black line is the sum of the other terms in the moisture budget.

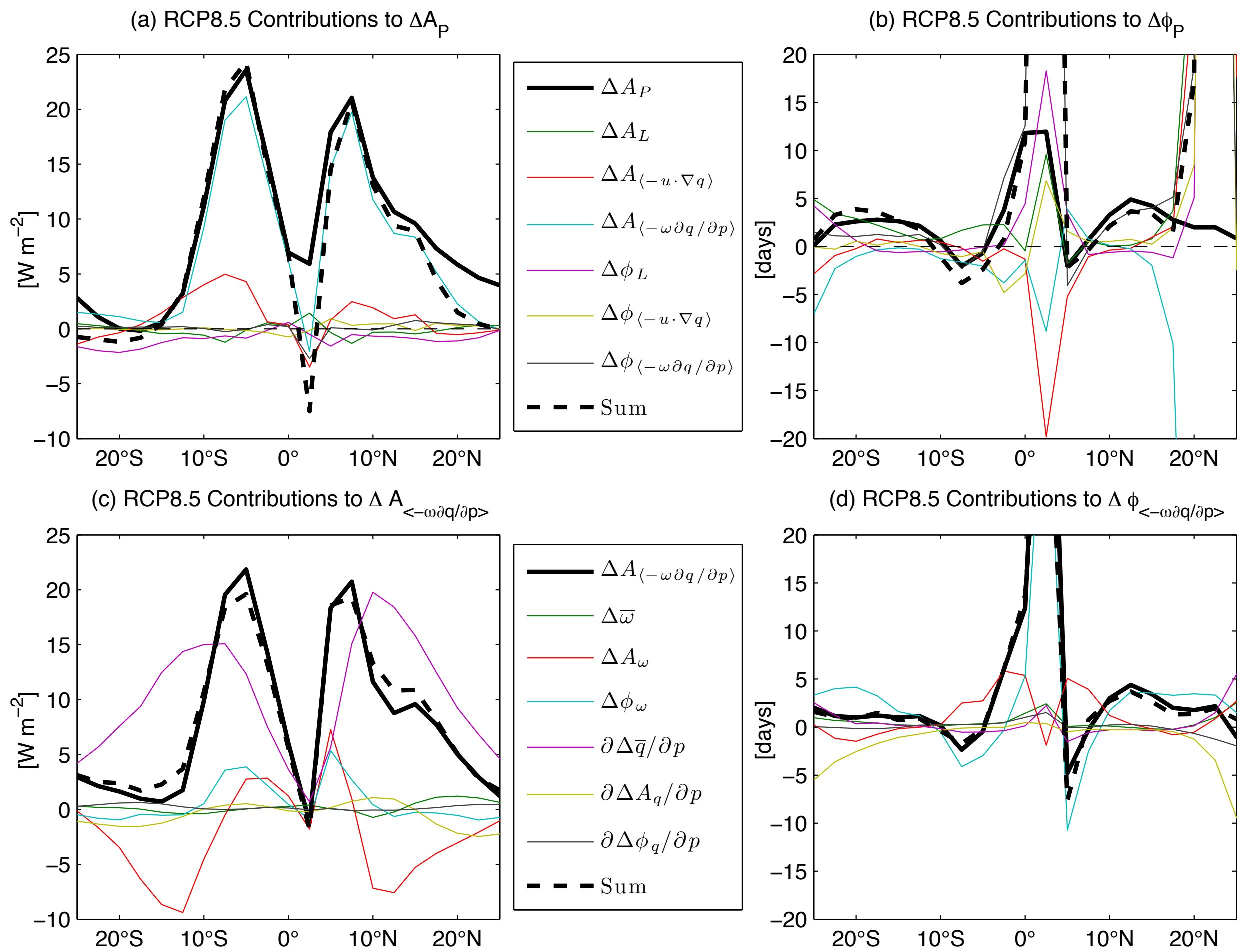

FIG. 5. Contributions of terms to ΔA_P (a) in the RCP8.5 CMIP5 simulation as well as ΔA_P itself (solid, thick, black line). The contribution of each term is the change in amplitude or phase multiplied by an appropriate factor (see appendix). The sum of the contributions is given by the dashed, thick, black line. As in (a), but for $\Delta\phi_P$ (b). We further decompose $\Delta A_{\langle -\omega \frac{\partial q}{\partial p}\rangle}$ (c) and $\Delta\phi_{\langle -\omega \frac{\partial q}{\partial p}\rangle}$ (d) into changes related to the annual mean, amplitude, and phase of ω and $\partial q/\partial p$.

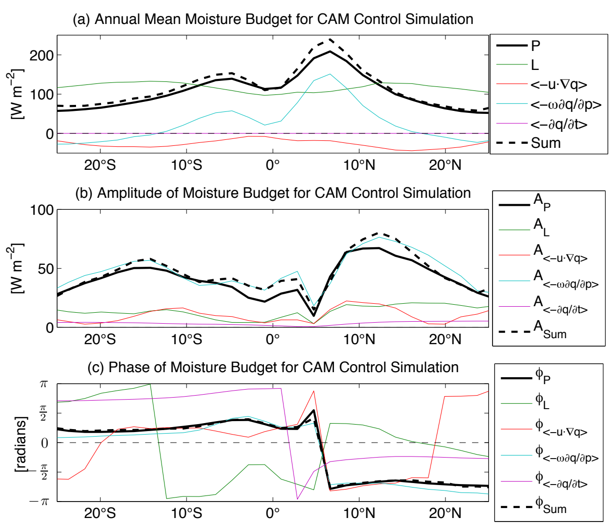

FIG. 6. As in Figure 4, but for the AGCM control simulation for the annual mean (a), amplitude (b), and phase (c) of precipitation.

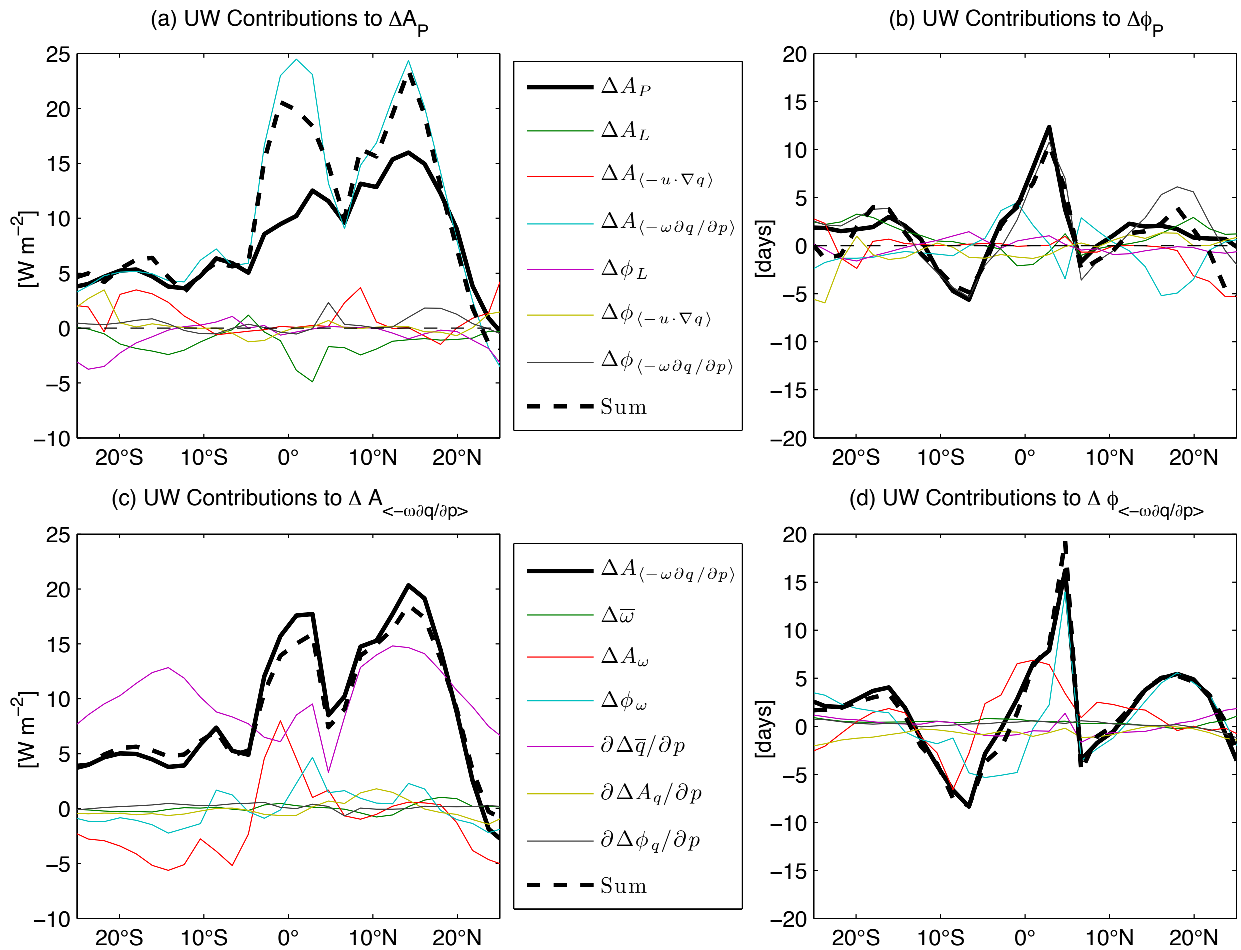

FIG. 7. As in Figure 5, but for the UW simulation. Contributions to (a) ΔA_P, (b) $\Delta\phi_P$, (c) $\Delta A_{\langle -\omega\frac{\partial q}{\partial p}\rangle}$, and (d) $\Delta\phi_{\langle -\omega\frac{\partial q}{\partial p}\rangle}$.

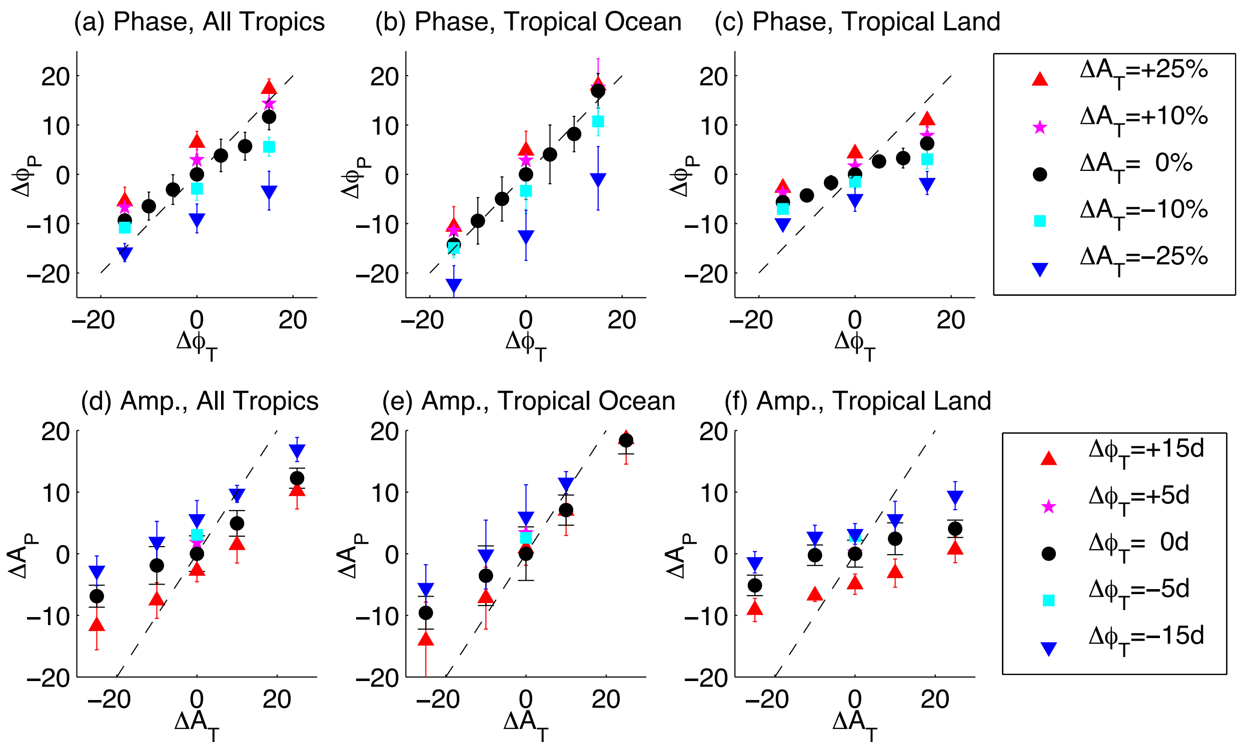

FIG. 8. Results of AGCM simulations with seasonality of precipitation as a function of imposed seasonality of SST. We plot the phase of precipitation against the phase of SST for the entire tropics (a), tropical ocean (b), and tropical land (c), with the colors representing the imposed amplitude of SST for each simulation. Similarly, we plot the amplitude of precipitation against the amplitude of SST for the entire tropics (d), tropical ocean (e), and tropical land (f), with colors representing the imposed phase of SST. Error bars represent one standard error.

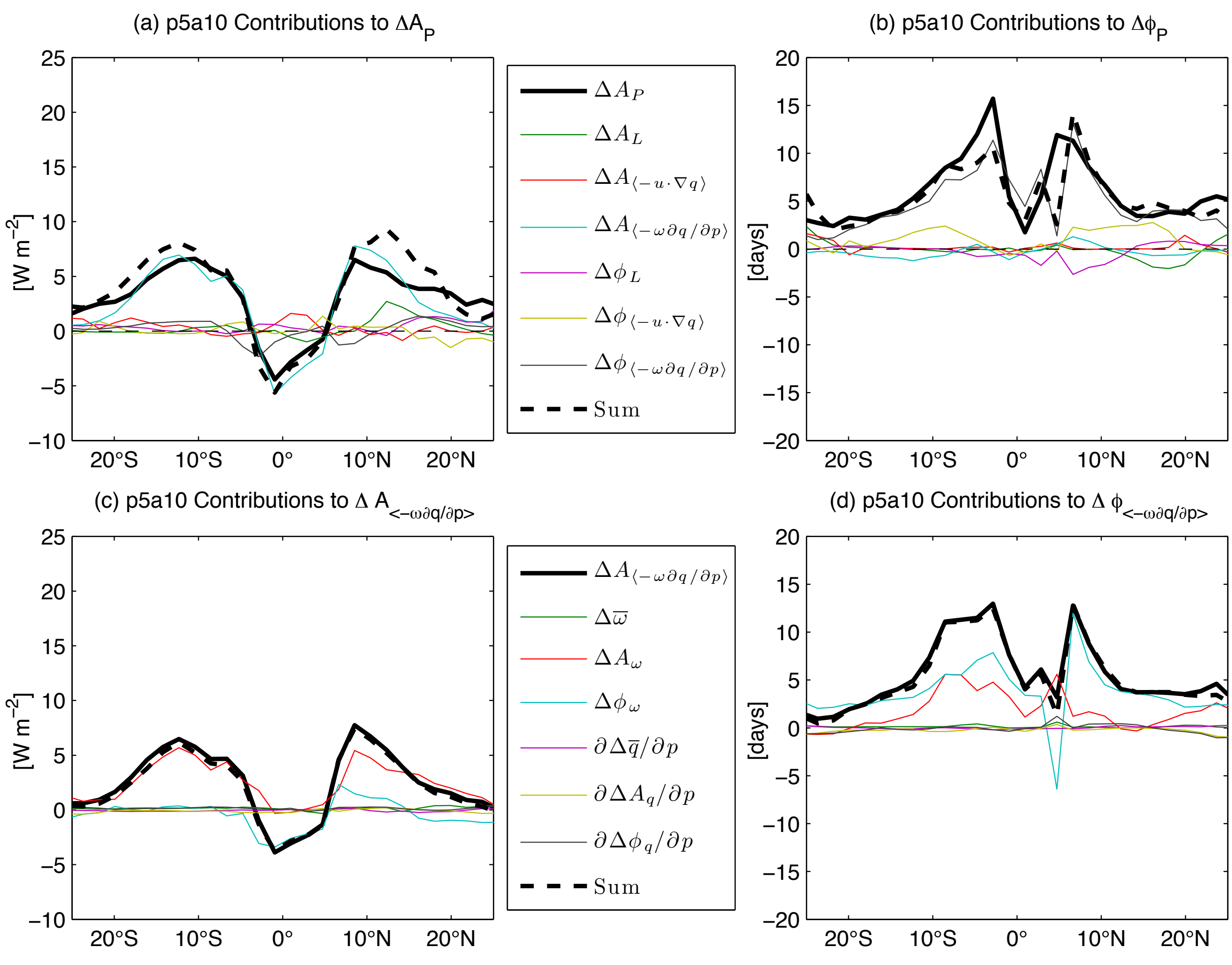

FIG. 9. As in Figure 7, but for the p5a10 experiment. Contributions to (a) ΔA_P, (b) $\Delta\phi_P$, (c) $\Delta A_{\langle -\omega\frac{\partial q}{\partial p}\rangle}$, and (d) $\Delta\phi_{\langle -\omega\frac{\partial q}{\partial p}\rangle}$.

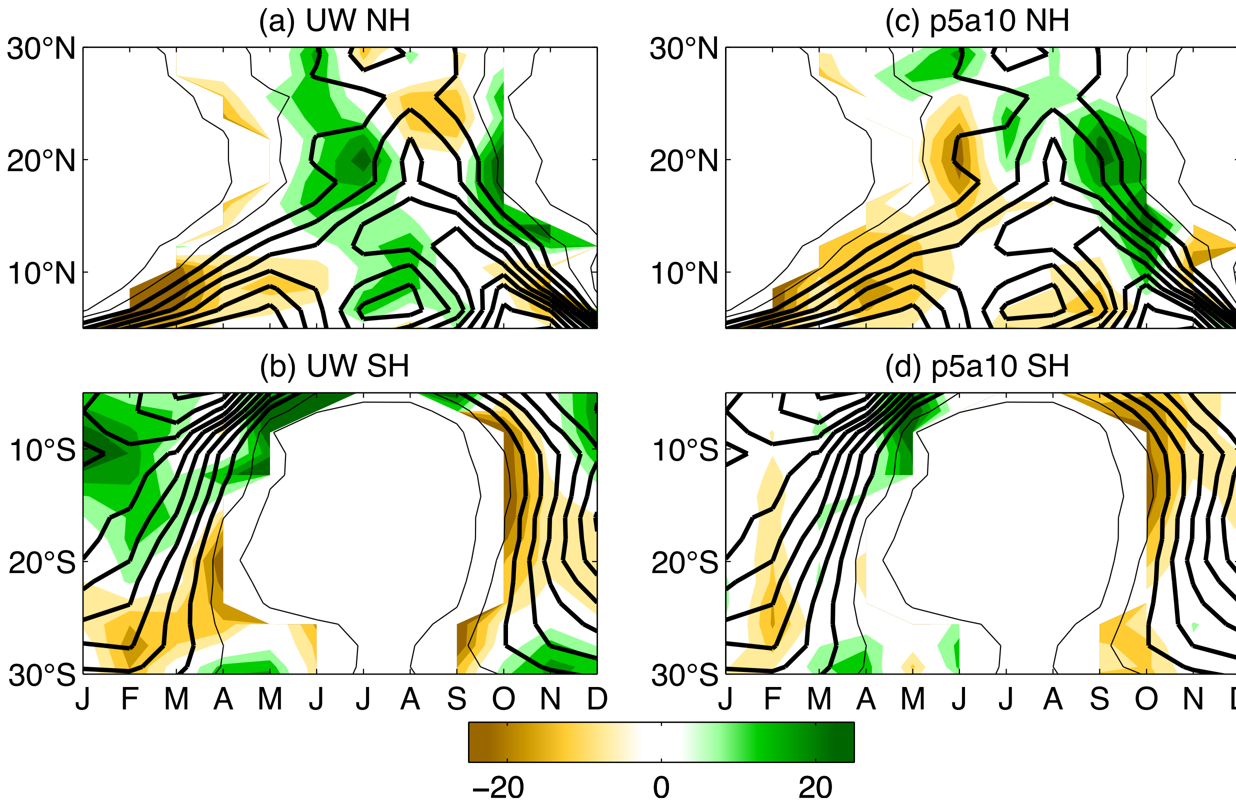

FIG. 10. Precipitation in land monsoon regions as a function of season and latitude in the control run (contour lines) and the percentage change (shading) for the UW simulation (a, b) and for the p5a10 simulation (c, d). In computing precipitation for NH monsoons (a, c) and SH monsoons (b, d), ocean has been masked out. Contour lines are at 1 mm day^{-1} intervals with thick contours representing precipitation of at least 3 mm day^{-1}. The precipitation change is not shown for regions where the precipitation in the control run is less than 1 mm day^{-1}.